

Article

Nitrogen Deficiency-Dependent Abiotic Stress Enhances Carotenoid Production in Indigenous Green Microalga *Scenedesmus rubescens* KNUA042, for Use as a Potential Resource of High Value Products

Seung-Woo Jo ^{1,†}, Ji Won Hong ^{2,†} , Jeong-Mi Do ^{3,4} , Ho Na ^{3,4}, Jin-Ju Kim ³,
Seong-Im Park ^{3,4}, Young-Saeng Kim ^{5,*}, Il-Sup Kim ^{6,*}  and Ho-Sung Yoon ^{1,3,4,6,*}

¹ Department of Energy Science, Kyungpook National University, Daegu 41566, Korea; jsw8796@gmail.com

² Department of Hydrogen and Renewable Energy, Kyungpook National University, Daegu 41566, Korea; jwhong@knu.ac.kr

³ Department of Biology, College of Natural Sciences, Kyungpook National University, Daegu 41566, Korea; leciel631@naver.com (J.-M.D.); myrambo10@naver.com (H.N.); deenamon@naver.com (J.-J.K.); sheep91528@naver.com (S.-I.P.)

⁴ School of Life Sciences, BK21 Plus KNU Creative BioResearch Group, Kyungpook National University, Daegu 41566, Korea

⁵ Research Institute of Ulleung-do and Dok-do, Kyungpook National University, Daegu 41566, Korea

⁶ Advanced Bio-resource Research Center, Kyungpook National University, Daegu 41566, Korea

* Correspondence: kyslhh1228@hanmail.net (Y.-S.K.); 92kis@hanmail.net (I.-S.K.); hsy@knu.ac.kr (H.-S.Y.); Tel.: +82-53-950-5348 (H.-S.Y.); Fax: +82-53-951-7398 (H.-S.Y.)

† These authors contributed equally to this work.

Received: 30 April 2020; Accepted: 2 July 2020; Published: 6 July 2020



Abstract: The microalgal strain *Scenedesmus rubescens* KNUA042 was identified in freshwater in Korea and characterized by evaluating its stress responses in an effort to increase lipid and carotenoid production. Under a two-stage cultivation process, the algal strain that generally exhibits optimal growth at a nitrate (source of nitrogen) concentration of 0.25 g L⁻¹ was challenged to different exogenous stimuli—salinity (S), light intensity (L), combined L and S (LS), and nitrogen deficiency (C)—for 14 days. Lipid production and carotenoid concentration increased in a time-dependent manner under these physicochemical conditions during the culture periods. Lipid accumulation was confirmed by thin layer chromatography, BODIPY staining, and fatty acid composition analysis, which showed no differences in the algal cells tested under all four (C, S, L, and LS) conditions. The quality of biodiesel produced from the biomass of the algal cells met the American Society for Testing and Materials and the European standards. Total carotenoid content was increased in the LS-treated algal cells (6.94 mg L⁻¹) compared with that in the C-, S-, and L-treated algal cells 1.75, 4.15, and 1.32 mg L⁻¹, respectively). Accordingly, the concentration of canthaxanthin and astaxanthin was also maximized in the LS-treated algal cells at 1.73 and 1.11 mg g⁻¹, respectively, whereas lutein showed no differences in the cells analyzed. Conversely, chlorophyll *a* level was similar among the C-, S-, and LS-treated algal cells, except for the L-treated algal cells. Thus, our results suggested that *S. rubescens* KNUA042 was capable of producing carotenoid molecules, which led to the maximum values of canthaxanthin and astaxanthin concentrations when exposed to the combined LS condition compared with that observed when exposed to the salinity condition alone. This indicates that the algal strain could be used for the production of high-value products as well as biofuel. Furthermore, this article provides the first evidence of carotenoid production in *S. rubescens* KNUA042.

Keywords: *Scenedesmus rubescens* KNUA042; biofuel; carotenoids; astaxanthin; nitrogen shortage

1. Introduction

Scenedesmus from the order Chlorococcales belongs to the family Scenedesmaceae and is frequently found to be dominant in freshwater bodies such as lakes and rivers. Worldwide, many species of this genus are used for various commercial purposes due to their rapid growth, ease of cultivation and handling, and ability to adapt to harsh environmental conditions [1]. Among them, *Scenedesmus* sp. has the potential to address the challenge of renewable energy-related problems by making a significant contribution to meeting bioenergy demand, as well as to provide additional environmental benefits [2]. Several reports suggest that over 15,000 compounds, including fatty acids, sterols, phenolic compounds, terpenes, enzymes, polysaccharides, alkaloids, and flavonoids that are sources of new natural products, can be extracted from microalgae, with many potential applications in the field of biotechnology [3–5]. For instance, the green microalga *S. obliquus* has been used as a model organism to produce biofuel (biodiesel and bioethanol) and other industrially important co-products such as β -carotene, omega-3 fatty acids, and glycerol [4]. In particular, carotenoid-mediated antioxidant compounds play important roles against various diseases, including chronic inflammation, atherosclerosis, cancer, cardiovascular disorders, and aging processes. This explains their considerable commercial potential in medicine, food production, and the cosmetics industry [5].

Carotenoids, an essential component of all photosynthetic organisms, constitute a structural group of natural pigments, which are produced as food additives and feed supplements. Recently, the antioxidant properties of carotenoids have been reported. Carotenoids are efficient scavengers of reactive oxygen species (ROS), especially singlet molecular oxygen, and peroxy radicals, which prevent ROS-mediated lipid peroxidation. Further, they are capable of detoxifying excited triplet states, which play a critical role in the protective effects of photooxidation-induced damage in plants [6]. In addition, carotenoids function synergistically with tocopherol, and this combination is more effective than a single compound in the ROS neutralization process. The dominant carotenoids are α -carotene, β -carotene, lycopene, lutein, zeaxanthin, and cryptoxanthin. The structure of a carotenoid is the key determinant of their physical properties, chemical reactivity, and biological functions. Chemical features unique to each carotenoid are associated with involvement in the molecular microenvironment and biological function.

A discovery that played an important role in antioxidant activity by preventing ROS-induced oxidative damage triggered the synthesis of a new carotenoid structure and the commercial production of these compounds. However, carotenoid production is not restricted to plants, algae, and cyanobacteria, given that some fungi and nonphotosynthetic bacteria can also produce carotenoids, but animals cannot. Microalgae can accumulate carotenoids in up to 14% of the algal biomass; these are classified as primary and secondary carotenoids [6]. Primary carotenoids are critical for photosynthesis, whereas secondary carotenoids that accumulate in the cytoplasmic lipid vesicles function with acquired tolerance to environmental conditions, including a range of abiotic and biotic stresses [7,8]. *Haematococcus pluvialis*, *Chlorella zofingiensis*, *C. photothecoides*, *Dunaliella salina*, and *S. almeriensis* are major carotenoid-producing microalgae. Accordingly, microalgae-based biotechnology for the production of these carotenoids is advantageous to several industries, including food, cosmetics, and pharmaceuticals [9,10].

Microalgae have attracted significant attention as a promising sustainable source of lipids and carotenoids and are capable of increasing production under abiotic stresses such as high salinity, light intensity, iron concentration, extreme temperatures, or nutrient limitation [11,12]. For instance, lipid accumulation in *Dunaliella* sp. and *C. vulgaris* increased by up to 70% and 21.1%, respectively, under high salinity conditions [13–15]. However, stress-based strategies usually influence cell growth in an adverse manner, causing ROS-induced oxidative damage and, eventually, reduced yields of the desired products [11,12]. In order to mitigate these drawbacks, alternative two-stage cultivation (TSC) strategies are used to enable the co-production of lipids and high-value products. In the TSC process, the first stage is dedicated to optimizing the growth conditions for maximum biomass yield, whereas the second stage focuses on increasing the concentration of lipids and carotenoids. This latter step is

achieved by creating unfavorable environmental conditions such as nutrient starvation (for example, through nitrogen (N) and phosphorus (P) limitation) or extreme exogenous stimuli. For instance, in biofuel production relying on *Isochrysis galbana*, the first growth stage occurs under abundant nutrient conditions such as increased algal biomass; then, cells are exposed to low salinity stress, resulting in an increase in the lipid content of up to 47% in the algal strain [16]. Consequently, a means of increasing biomass by TSC was developed to mitigate the negative effects of a stress-based manipulation. However, because TSC involves complex processes, it is important to develop new production strains that are capable of optimal growth under extreme stress conditions. Thus, the most viable strategy is to develop locally adapted algal strains.

In this study, we used modified TSC-dependent physiological responses against abiotic stress using in *S. rubescens* KNUA042, a novel eukaryotic microalgal strain isolated from freshwater in Korea, for the synchronized production of combined metabolites (i.e., long-chain, fatty-acid-derived lipids and carotenoids) rather than a single metabolite.

2. Materials and Methods

2.1. Isolation and Identification of *S. rubescens* KNUA042 from Freshwater

Freshwater samples collected in May 2017 from a puddle on Dokdo island (37°14′19.8″ N 131°52′09.3″ E) in Korea were inoculated into 100 mL of BG-11 medium supplemented with 100 µg mL⁻¹ imipenem (JW Pharmaceutical, Seoul, Korea) in 250-mL flasks to obtain an axenic strain and then incubated at 25 °C under cool fluorescent light (approximately 100 µmol m⁻² s⁻¹), 16 h light/8 h dark cycle, and 0.2-µm pore antibacterial air filters until algal growth was apparent [17]. Then, the algal biomass from well-grown algal cultures was harvested by centrifugation (6000 rpm, 3 min, 25 °C). The compositions (g L⁻¹) of the BG-11 medium used were as follows: 1.5 sodium nitrate (NaNO₃), 0.04 dipotassium phosphate dehydrate·2H₂O, 0.075 magnesium sulfate heptahydrate·7H₂O, 0.036 calcium chloride·2H₂O, 0.006 citric acid, 0.02 sodium carbonate, 0.006 ferric ammonium citrate, 0.001 sodium-ethylenediaminetetraacetic acid, and 1 mL of the trace metal A5. The trace metal A5 solution (g L⁻¹) comprised 2.86 boric acid, 1.81 manganese chloride tetrahydrate, 0.22 zinc sulfate·7H₂O, 0.39 sodium molybdate·2H₂O, 0.079 copper sulfate pentahydrate, and 0.05 cobalt chloride hexahydrate.

The resulting cell pellets were streaked onto an R2A agar medium (BD Biosciences, San Jose, CA, USA) and incubated under the identical conditions as described above. A single colony was selected and aseptically restreaked onto a fresh R2A agar medium. Then, to obtain an axenic culture, the growth from a single colony was inoculated into BG-11 medium without antibiotics and cultured at 25 °C on an orbital shaker (Vision Scientific Korea, Bucheon, Korea) with shaking at 160 rpm. Cultured cells were harvested by centrifugation at 6000 rpm for 3 min, washed twice with deionized distilled water, observed at 1000 × using a light microscope (Zeiss Axio Imager A2; Carl Zeiss, Göttingen, Germany), and captured by an AxioCam MRc camera equipped with Zen 2.3 software. Microalgae identification at the molecular level included the following. Genomic DNA was isolated from the algal cells using the Qiagen DNeasy Plant Mini kit according to the manufacturer's instructions (Qiagen, Hilden, Germany). Polymerase chain reaction (PCR) was performed with universal primer sets of 18S rRNA, *rbcL*, and ITS2 regions, as described previously [18,19]. Purified PCR amplicons were ligated into the pGEM T-Easy vector (Promega, Madison, WI, USA), according to manufacturer's instructions. The resulting constructs were transformed into *Escherichia coli* DH5α, amplified, and sequenced. Closely matched sequences of 18S rRNA, *rbcL*, and ITS2 were confirmed using the NCBI blast and aligned using the MEGA 7.0 software [20].

2.2. Microalgal Cultivation Conditions

Seed cultures of the microalgae were harvested by centrifugation (4000 rpm, 5 min, 25 °C) when optical density reached approximately 1.2 at 680 nm. The algal cell pellets were inoculated in fresh BG-11 medium (adjusted to 100 mL of final volume) supplemented with different concentrations of

NaNO₃ (0, 25, 50, and 250 mg L⁻¹) as the N source, and cultured at 25 °C on an orbital shaker with shaking at 160 rpm under cool fluorescent light (approximately 100 μmol m⁻² s⁻¹ and a 16 h light/8 h dark cycle). The BG-11 medium and aeration conditions were identical to those mentioned above. Following cultivation for 14 days, the algal cells were exposed to abiotic stresses—S (400 mM NaCl), L (1000 μmol m⁻² s⁻¹), and combination L and S (LS), and N deficiency(C)—for an additional 14 days.

2.3. Algal Growth Kinetics, Biomass Productivity, and N Consumption

Microalgae growth rates were monitored by measuring optical density (A₆₈₀) at 2-day intervals for the indicated time using a spectrophotometer (Optimizer 2120 UV spectrophotometer; Mecasys, Daejeon, Korea). Algal biomass productivity was determined by measuring the dry weight using the gravimetric method, as reported previously [21]. Briefly, 10 mL of culture solution was filtered through GE Healthcare GF/C Whatman™ filter paper (0.7 μm pore size; Thermo Fisher Scientific, Leicestershire, UK) and incubated at 105 °C for 24 h in a drying oven. The dried filters were cooled at 25 °C, and reweighed. Dry weights were calculated by subtracting the filter weight from the total weight. The nitrate concentration of the sample was measured using the HS-NO₃(CA) water testing kit (Humas, Daejeon, Korea).

2.4. Characterization of Microalgal Biomass

The harvested biomass was freeze-dried using a freeze dryer (PVTFD20R; Ilshin Lab, Suwon, Korea), pulverized with a mortar and pestle, and sieved through an American Society for Testing and Materials (ASTM) No. 230 mesh (mesh pore size 63 μm). Total lipid content was determined according to the colorimetric sulfo-phosphor-vanillin, as described previously [22]. During proximate analysis, approximately 10 mg of the sample was used to measure the ash content using a thermal analyzer (DTG-60A; Shimadzu, Kyoto, Japan). Alpha-alumina (α-Al₂O₃) powder (30 mg) was introduced as a reference. During this process, nitrogen (N₂) gas was supplied at a rate of 25 mL min⁻¹ to protect the microalgae powder from oxidation, and the samples were heated from 50 to 900 °C at a rate of 10 °C min⁻¹. Thermogravimetric analysis (TGA) was conducted using the TA60 version 2.21 software (Shimadzu). In addition, an ultimate analysis was also conducted to determine the carbon (C), hydrogen (H), nitrogen (N), and sulfur (S) contents using an elemental analyzer (Flash 2000; Thermo Fisher Scientific, Milan, Italy). The oxygen (O) content was calculated by subtracting the contents of ash and CHNS from the total contents. Higher heating value (HHV) was calculated using a formula developed by Given et al. [23].

$$\text{HHV} = \{0.3278\text{C} + 1.419\text{H} + 0.09257\text{S} - 0.1379\text{O} + 131\text{N} + 0.637 \text{ (MJ/kg)}\} \quad (1)$$

2.5. Thin Layer Chromatography and BODIPY Staining

Lipid extraction was performed using the method developed by Breuer et al. [24]. The extracted crude lipids (approximately 20 μL) were mixed with n-hexane/diethyl ether (3:1, v/v). This mixture was then used for thin-layer chromatography (TLC) analysis (silica gel 60 F254, 10 × 10 cm, 0.25 mm thickness; Merck, Germany). Glyceryl trioleate (0.2 mg) was used as a reference for relative lipid quantitation. Following TLC-based separation, the neutral lipids were reversibly stained using iodine vapor at 37 °C for 10 min. The visualized signal intensity was determined using the ImageJ software. Lipids were stained with the lipophilic fluorescent dye BODIPY 505/515 (4, 4-Difluoro-1, 3, 5, 7-tetramethyl-4-bora-3a, 4a-diaza-s-indacene; Invitrogen™, Fisher Scientific, Carlsbad, CA, USA) adjusted to a final concentration of 1 mM in 0.1% dimethyl sulfoxide [25]. Images of green BODIPY fluorescence were obtained using an inverted confocal laser scanning microscope (LSM 700; Carz Zeiss, Germany) under excitation with a 488 nm laser line and emission at 505–515 nm using a band-pass filter [25].

2.6. Pigment Analysis

The culture solution (2 mL) was centrifuged at 13,000 rpm for 5 min. The harvested cell pellets were resuspended in 2 mL of absolute ethanol, then extracted in an ice bath using a probe-type sonicator (Branson Ultrasonics™ Sonifier™ 450; Fisher Scientific, Ottawa, Ontario, USA). The extracted liquid solution was incubated at 4 °C for 24 h in the dark and centrifuged at 13,000 rpm for 5 min. The cleared supernatant was measured using a UV–VIS spectrophotometer at 470, 649, and 664 nm, as reported previously [26]. The pigment amounts were determined by the following equations:

$$\text{Chlorophyll } a \text{ (Chl } a) = 13.36A_{664} - 5.19A_{649} \quad (2)$$

$$\text{Chlorophyll } b \text{ (Chl } b) = 27.43A_{649} - 8.12A_{664} \quad (3)$$

$$\text{Total carotenoid (Car)} = (1000A_{470} - 2.13 \text{ Chl } a - 97.63 \text{ Chl } b)/209 \quad (4)$$

The extracted crude solution was filtered through a 0.2- μm membrane filter (Minisart® syringe filter, Sartorius Stedim Biotech, Gottingen, Germany). Samples were mixed with high-performance liquid chromatography (HPLC) grade H₂O (Daejung, Siheung, Korea). To avoid peak distortion, 40 μL of HPLC grade H₂O was added to 200 μL of each sample extract immediately prior to injection [27]. Samples were then analyzed on an Agilent 1260 Infinity HPLC system (Waldbronn, Germany) equipped with a Discovery C18 column (25 cm \times 4.6 mm, 5 μm , Supelco, Bellefonte, PA, USA) at 33 °C. Pigment profiles were detected and quantified by measuring absorbance at 440 nm. The mobile phase gradient was programmed as described by Sanz et al. [28] at a constant flow rate of 1 mL min⁻¹, with a mixture of methanol:ammonium acetate (82:18, v:v) used as solvent A, and ethanol as solvent B. For carotenoid analysis, undiluted samples were analyzed with a C30 carotenoid column (25 cm \times 4.6 mm, 5 μm , YMC, Kyoto, Japan) at 25 °C. Astaxanthin, lutein, and canthaxanthin were detected and quantified by absorbance at 474 nm. The mobile phase comprised methanol/methyl tert-butyl ether/H₂O in the ratio of 81:15:4 (v:v:v) at a constant flow rate of 1 mL min⁻¹ for 45 min. Pigment standards (astaxanthin, canthaxanthin, chlorophyll *a*, chlorophyll *b*, lutein, and β -carotene) were purchased from Sigma-Aldrich (St. Louis, MO, USA). Pigment content was quantified by calculating the total peak areas of each pigment derived from a calibration curve.

2.7. Fatty acid Analysis

Fatty acid methyl ester (FAME) composition was analyzed using a gas chromatograph mass spectrometer (GC/MS 7890A; Agilent, Santa Clara, CA, USA) equipped with a mass selective detector (5975C; Agilent) and the DB-FFAP column (30 m, 250 μm ID, 0.25 μm film thickness; Agilent). The initial temperature was 50 °C and maintained for 1 min. The temperature was increased to 200 °C at a rate of 10 °C min⁻¹ for 30 min, then increased to 240 °C at a rate of 10 °C min⁻¹, and held for 20 min. The injection volume was 1 μL , with a split ratio of 20:1. Helium gas was supplied at a constant flow rate of 1 mL min⁻¹. For the mass spectrometer parameters, injector and source temperatures were 250 and 230 °C, respectively, and the electron impact mode at an acceleration voltage of 70 eV was used for sample ionization, with an acquisition range of 50–550 mass to charge ratio [29]. Compounds were identified by matching their mass spectra with the Wiley/NBS libraries.

2.8. Assessment of Biodiesel Quality

The quality of biodiesel was determined by assessing the saponification value (SV), iodine value (IV), degree of unsaturation (DU), cetane number (CN), cold filter plugging point (CFPP), oxidation stability (OS), kinematic viscosity (ν), and density (ρ), which were calculated based on the fatty acid composition using the following empirical equations, as reported previously [30,31].

$$\text{SV} = \sum \frac{560 \times \text{N}}{\text{M}} \quad (5)$$

$$IV = \sum \frac{254 \times N \times D}{M} \quad (6)$$

$$CN = \left(46.3 + \frac{5458}{SV}\right) - (0.225 \times IV) \quad (7)$$

$$CFPP = (3.1417 \times LCSF) - 16.477 \quad (8)$$

$$DU = MUFA + (2 \times PUFA) \quad (9)$$

$$OS = \frac{117.9295}{x} + 2.5905 \quad (0 < 100) \quad (10)$$

$$v = -12.503 + 2.496 \times \ln(MW) - 0.178 \times N \quad (11)$$

$$\rho = \sum 0.8463 + \frac{4.9}{MW} + 0.0118 \times N \quad (12)$$

D, M, and N represent the number of double bonds, the average molecular mass, and the content (wt%) of each fatty acid, respectively. MUFA and PUFA indicate the content of the monounsaturated fatty acids and polyunsaturated fatty acids, respectively.

2.9. Statistical Analysis

All experiments were performed in triplicate. Data shown are presented as the average of the triplicates, and error bars represent the standard deviation (SD). Statistical analysis was conducted using the SPSS software. Lipid content, biomass, and lipid productivity were statistically tested using one-way analysis of variance (ANOVA) and post-hoc Tukey's honestly significant difference (HSD) test. *p* values of < 0.05 were considered statistically significant.

3. Results

3.1. Identification of *S. rubescens* KNUA042

The KNUA042 strain was isolated from axenic algae cultures obtained from a freshwater puddle in a cave in Korea's eastern Dokdo islands (37°14'19.8" N 131°52'09.3" E) (Figure S1A,B). Preliminary morphological analysis showed that the KNUA042 cells were round with a slightly ellipsoid shape and nonmotile with diameters of 6–10 μm. Cytological analysis revealed that the algal KNUA042 strain possessed a chloroplast comprising one pyrenoid that was divided into two cells at the vegetative stage (Figure S1C). Based on these morphological results, the algal KNUA042 was very similar to *Scenedesmus rubescens* reported by Kessler et al. [32]. AlgaeBase, the primary compilation of algal names list *S. rubescens* as a synonym of *Halochlorella rubescens*. *Scenedesmus* is one of the most common freshwater algae genera; however, the extremely diverse morphologies found within species make its identification difficult. Thus, we used PCR-based molecular analysis for identification. The nucleotide sequences of the 18S rRNA, ITS2, and *rbcl* genes were obtained and compared with published green algal sequences. BLAST hits for the ITS2 (426 bp), and 18S rRNA (1767 bp) genes shared 99% identity with *S. rubescens* KMMCC 263 (accession no. JQ315585), and *Scenedesmus* sp. SM8_2 (accession no. KT778097), respectively (Table S1). In phylogenetic tree analysis using ITS2 and 18S rRNA, KNUA042 belonged to a member of *Scenedesmus* sp. (Figure S2) and *S. rubescens*, respectively (Figure S3). Specifically, the 18S rRNA sequence indicated a close relationship with the green algae *S. rubescens*. Thus, the KNUA042 strain displayed the highest sequence relatedness with the green algae, *S. rubescens* (100% similarity). The genus *Scenedesmus* is a member of the family Scenedesmaceae. In nucleotide sequences produced *rbcl* (1385 bp), the algal strain was searched as *Acutodesmus* sp. (HQ246361) (Table S1). However, the morphology of the isolated microalgae was very disparate from *Acutodesmus* sp. Taken together, the KNUA042 strain displayed the highest sequence relatedness with the green algae *S. rubescens* (100% similarity).

3.2. The Effect of Nitrate on *S. rubescens* KNUA042

The effect of nitrate concentration on growth was examined by culturing the microalgal *S. rubescens* KNUA042 strain in BG-11 medium containing various concentrations of NaNO_3 (0, 25, 50, and 250 mg L^{-1}) as an N source. Algal cells grown in the medium supplemented with 25 and 50 mg L^{-1} NaNO_3 almost exhausted on the 14th and 23rd days, respectively, after inoculation, whereas the algal cells treated with 250 mg L^{-1} NaNO_3 were consumed approximately 180 mg L^{-1} under the same culture conditions (Figure S4A). Next, the relationship between N uptake and cell growth was examined by measuring the dry weight and optical density, and a slight difference was noted in the dry weight for all analyzed samples, whereas the optical density showed a promising distinction, with absorbance being the highest for the 50 mg L^{-1} -treated algal cells than that for the other cells (Figure S4B,C). We found a correlation between dry weight and optical density at >97% (Figure S4D). Furthermore, this purpose established a platform for the production of algal biomass-based lipids and carotenoids produced by *S. rubescens* KNUA042. Thus, to manipulate a mass culture to yield biomass with the desired products, including fatty acid, lipids, and carotenoids, subsequent experiments were performed with 25 mg L^{-1} NaNO_3 rather than that of 50 mg L^{-1} NaNO_3 . Figure 1 depicts the growth kinetics, N consumption, and dry weight of the algal KNUA042 cells grown in BG-11 medium supplemented with 25 mg L^{-1} NaNO_3 . All values analyzed were time-dependent during the culture periods. N consumption was completely depleted on the 14th day of culture, with an optical density and dry weight of 0.939 and 0.35 g L^{-1} , respectively. In the algal cells grown in BG-11 medium supplemented with 50 and 250 mg L^{-1} , the remaining concentration of NaNO_3 was 5.66 and 125.64 mg L^{-1} , respectively, during the same culture time (Figure S4A). Thus, potentially the 25 mg L^{-1} -mediated N limitation produced by *S. rubescens* KNUA042 affected the biochemical pathways of the algal cells and indirectly increased lipid productivity and high-value products.

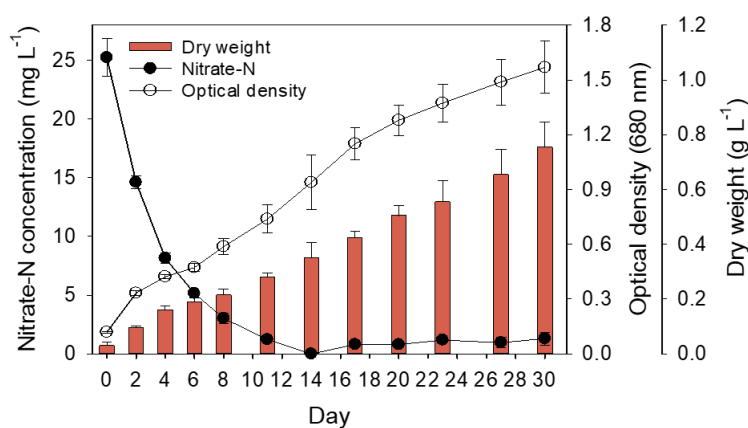


Figure 1. Nitrate–N concentration, optical density, and dry weight of *S. rubescens* cultures under light at $100 \mu\text{mol m}^{-2} \text{s}^{-1}$ at 25°C from day 0 to day 30. Each measurement indicates mean \pm SD of triplicates.

3.3. Productivity of Lipids and Biomass under Abiotic Stress Plus N Deficiency

Lipid content and biomass productivity were estimated when the algal KNU042 cells were exposed to abiotic stress in the presence of N deficiency. Algal cells were grown in BG-11 medium supplemented with 25 mg L^{-1} NaNO_3 for 14 days at 25°C under four culture conditions: control without stressor (C; N deficiency), high salinity (S; 400 mM NaCl), high light intensity (L; $1000 \mu\text{mol m}^{-2} \text{s}^{-1}$), and combined stress (light intensity and salinity; LS). These cells were then cultured at 25°C for an additional 14 days. As shown in Figure 2, dry weight increased in a time-dependent manner during the additional culture periods, which corresponded to the changes in lipid content and lipid productivity. Specifically, lipid content and dry weight were higher in the combined LS-treated cells ($42.99\% \pm 0.72\%$ and $1.13 \pm 0.05 \text{ g L}^{-1}$, respectively) than in the single-stress-treated cells—C ($38.14\% \pm 0.82\%$ and $0.86 \pm 0.01 \text{ g L}^{-1}$, respectively), S ($38.47\% \pm 0.88\%$ and $1.03 \pm 0.06 \text{ g L}^{-1}$,

respectively), and L ($33.62\% \pm 1.72\%$ and $0.85 \pm 0.01 \text{ g L}^{-1}$, respectively) (Figure 2A,B). In addition, the combined LS stress led to maximum biomass productivity ($80.71 \pm 4.40 \text{ mg L}^{-1} \text{ d}^{-1}$) and lipid productivity ($34.75 \pm 1.64 \text{ mg L}^{-1} \text{ d}^{-1}$) on the 14th day of culture. In the C- and L-treated cells, there was no difference in biomass and lipid productivity; furthermore, biomass and lipid productivity in the C- (61.78 ± 0.50 and $23.41 \pm 0.15 \text{ mg L}^{-1} \text{ d}^{-1}$, respectively) and L-treated cells (60.71 ± 0.01 and $20.21 \pm 0.18 \text{ mg L}^{-1} \text{ d}^{-1}$, respectively) was lower than that in the S (73.92 ± 4.54 and $28.51 \pm 2.01 \text{ mg L}^{-1} \text{ d}^{-1}$) and LS-treated cells (80.71 ± 4.04 and $34.76 \pm 1.64 \text{ mg L}^{-1} \text{ d}^{-1}$, respectively) (Figure 2C). Thus, our results show that maximum lipid productivity is produced under combined conditions in which physicochemical stresses (salinity + light intensity) are coupled N deficiency in *S. rubescens* KNUA042.

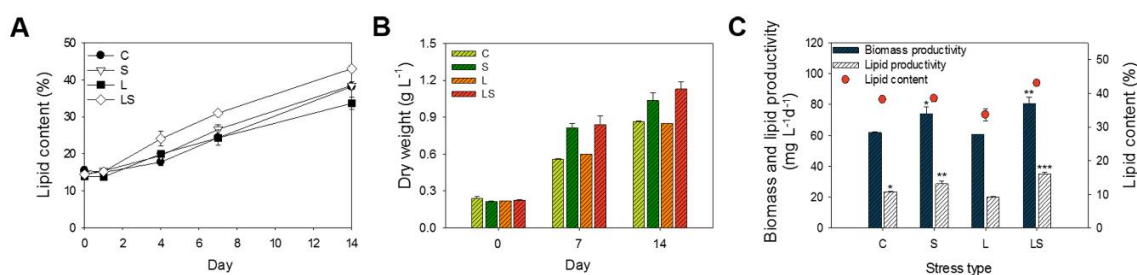


Figure 2. (A) Lipid content and (B) dry weight of *S. rubescens* culture cells under different stress conditions from day 0 to day 14. (C) Comparison of biomass, lipid productivity, and lipid content obtained from *S. rubescens* KNUA042 grown under different stress conditions on the final day of cultivation. Values were presented as the mean \pm SD of triplicates. Significant differences compared with each other were analyzed by one-way ANOVA, post-hoc tests, and Tukey's HSD test (* $p < 0.05$, ** $p < 0.01$, *** $p < 0.005$, respectively). C, control (N deficiency); S, salinity (400 mM); L, high light intensity ($1000 \mu\text{mol m}^{-2} \text{ s}^{-1}$); LS, combined stimulation (light intensity + salinity).

3.4. BODIPY Staining, Cell Size and Triacylglycerol Accumulation at Different Environmental Conditions

Under N deficiency-dependent abiotic conditions, increased lipid productivity and lipid content was observed in *S. rubescens* KNUA042 cells, as depicted in Figure 2. Based on these results, the staining of neutral lipids from the microalgae was conducted using fluorescent BODIPY dye. From the BODIPY^{505/515}-mediated fluorescent signal intensity, S- and LS-treated algal cells exhibited a granular spatial fluorescence pattern compared with the C- and L-treated algal cells (Figure 3A). In addition, the sizes of the C- and L-treated algal cells were 2-fold smaller than those of the S- and LS-treated cells. The population of C- (3.41×10^6 cells) and L-treated algal cells (2.62×10^6 cells) was greater than that of the S- (1.96×10^6 cells) and LS-treated algal cells (1.97×10^6 cells). In contrast, mass per cell values were greater in the S- (0.52) and LS-treated algal cells (0.57) than in the C- (0.25) and L-treated algal cells (0.32) (Figure 3B). Therefore, cell mass was found to be inversely related to cell population under stress conditions. These results were supported by optical density-based growth kinetics; the growth rate was the highest in the C-treated cells, followed by the L-, S-, and LS-treated cells (Figure S5).

The present study determined triglycerides' (TAGs) intensity using TLC as in total lipid extracts and found that their intensities were enhanced under specific abiotic stresses—N deficiency, high salinity, high light intensity, and a combination of high light intensity and high salinity—as shown in Figure 3A. TAG content was determined in all algal cells after 4 days of stress exposure (C, S, L, and LS) and TAG accumulation was observed in a time-dependent manner (Figure S6A). The highest signal intensity from TAG content was observed in the 14-day S-treated algal cells, whereas the lowest signal intensity was detected in the 14-day L-treated algal cells (Figure S6B). Thus, our results indicated that high salinity accelerates cell weight and neutral lipid accumulation, including TAGs, whereas high light intensity reduces cell mass and lipid droplets. Furthermore, the combination of high salinity and high light intensity generated the highest cell weight and fluorescence intensity through a synergistic biochemical pathway in contrast to a single stress response.

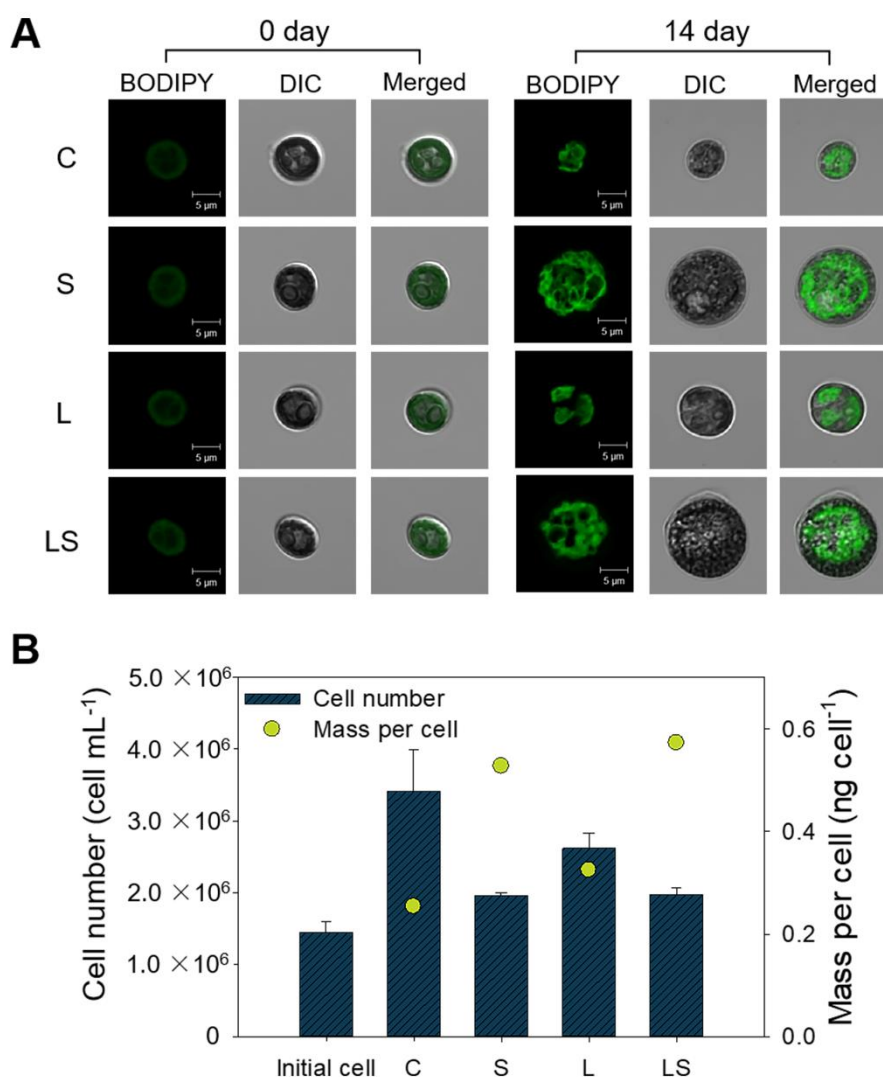


Figure 3. (A) Confocal microscopy images of BODIPY^{505/515}-stained *S. rubescens* KNUA042 cells under different stress conditions at days 0 and 14 of culture, with scale bar shown directly in each image. (B) Comparison of cell number and mass per cell under different stress conditions on the final day of cultivation. C, control (N deficiency); S, salinity (400 mM); L, high light intensity (1000 $\mu\text{mol m}^{-2} \text{s}^{-1}$); LS, combined stimulation (light intensity + salinity).

3.5. Proximate Analysis

Given that the biomass productivity and lipid content of algal cells were increased when exposed to abiotic stress, we performed a proximate analysis to estimate the composition of the algal biomass. The analysis of algal *S. rubescens* KNUA042 cells was based on three major components of biomass—moisture, volatile matter, and ash (Table 1). We found that the moisture and ash contents gradually decreased in a time-dependent manner under stress conditions. The initial moisture content of all the four-dependent unstressed-cells was approximately 6.3 ± 0.1 – 6.6 ± 0.2 weight percentage (wt%). When algal cells were challenged by a specific stress for 14 days, their moisture content decreased to 5.1 ± 0.3 , 4.9 ± 0.2 , 5.7 ± 0.4 , and 5.0 ± 0.3 wt% in the C-, S-, L-, and LS-treated cells, respectively. The moisture content of S- and LS-treated algal cells was <5 wt%. Ash contents were initially adjusted to 16.2 ± 0.2 – 18.2 ± 0.4 wt% and then decreased to 4.6 ± 0.2 – 6.6 ± 0.2 wt% in the stressed cells after 14 days, with the greatest decrease observed in the S-treated cells (4.6 ± 0.2 wt%). In contrast, the starting value of volatile matter in all algal cells was 75.5 ± 0.5 – 77.2 ± 0.4 wt% with these values increasing to final values of 88.2 ± 0.1 , 90.5 ± 0.0 , 87.9 ± 0.4 , and 89.2 ± 1.2 wt% in the C-, S-, L-, and LS-treated cells, respectively, at

14 days. Thus, proximate analysis of *S. rubescens* KNUA042 suggested that it has a low moisture content, high volatile matter, and moderate ash content, potentially making it a promising biomass fuel.

3.6. Ultimate Analysis

The C, N, H, O, and S contents were determined in ash biomass. Table 1 shows the C, H, N, and S proportions in ash biomass from the unstressed and stressed algal cells. No differences were found in the initial C (42.2 ± 0.2 – 42.9 ± 0.3 wt%), H (6.3 ± 0.1 – 6.4 ± 0.3 wt%), N (6.6 ± 0.1 wt%), S (0.5 ± 0.0 wt%), and O (25.9 ± 0.2 wt%) contents of algal cells prior to stress exposure. However, these values changed in a time-dependent manner during the 14-day stress treatment, although no substantial differences were observed in any algal cells tested initially (C-, S-, L-, and LS-treated cells). The C and H contents increased at 53.1 ± 0.1 – 55.1 ± 0.4 wt% and 8.1 ± 0.0 – 8.4 ± 0.1 wt%, respectively, while the N and S contents were decreased at 2.9 ± 0.0 – 3.2 ± 0.1 wt% and approximately 0.3 ± 0.0 wt%, respectively (Table 1). In contrast, the O content remained unchanged regardless of the abiotic stress applied and accounted for approximately 25.9 ± 0.2 wt% of the unstressed cells and 24.1 ± 0.5 – 26.3 ± 0.4 wt% of the stressed cells. Furthermore, the changes in C content amounted to an increase of 28.1%, 27.5%, 24.3%, and 28.4% in the C-, S-, L-, and LS-treated cells, respectively, relative to the unstressed cells. HHV also increased by up to 28.2%–34.6% in a time-dependent manner during stress exposure, with no differences found in the four algal cells tested. The initial HHV was [33,34] 20.0 ± 0.0 – 20.2 ± 0.2 MJ kg^{-1} , whereas the final HHV was 25.9 ± 0.0 – 27.2 ± 0.3 MJ kg^{-1} . The highest and lowest HHVs were observed in the LS- and L-treated cells, respectively.

3.7. Analysis of the Fatty Acid Composition to Abiotic Stress

To estimate the quality of microalgal fatty acids in TSCs following abiotic stress and N deficiency, we performed a GC-MS analysis of the fatty acids and identified C16:0 (palmitic acid), C18:1 (oleic acid), and C18:3 (linolenic acid), which together accounted for over 80% of the relative composition of fatty acids, as the major compounds (Figure 4A). The composition of C16:0 was adjusted at 15.91%–18.95% of the initial value and then increased time-dependently by 20.97%–29.05% during the 14-day stress exposure; this was highlighted in the L-treated algal cells (29.05%) and the LS-, C-, and S-treated algal cells. Initially, the composition of C18:1 was approximately 13% of the starting compositions, with accumulation resulting in an increase of 39.14%–46.40% under the equivalent final conditions. Microalgae accumulate lipids for long-term energy storage under unfavorable conditions, including the induction of oleic acid (C18:1) as part of the fatty acid composition, which is known to be typical during N starvation [35]. The values of lipid content in order were 46.40%, 44.20%, 42.24%, and 39.14% in the S-, C-, LS-, and L-treated algal cells, respectively. In contrast, the relative composition of C18:3 decreased over the experimental period to 39.16%–44.41% of the initial values, with final compositions, in experimental order being C- (12.11%), S- (12.60%), LS- (13.76%), and the L-treated algal cells (17.07%). Overall, prior to abiotic stress treatment, no differences were found in saturated-fatty acid (SFA), monounsaturated-fatty acid (MUFA), or polyunsaturated fatty acid (PUFA) composition in the algal cells (C-, S-, L-, and LS-treated cells); initially, the relative compositions of these fatty acid groups accounted for 16.21%–16.52%, 10.79%–12.12%, and 54.06%–54.58%, respectively (Figure 4B). Upon stress treatment, the content of SFA and MUFA accelerated in a time-dependent manner in the all algal cells, whereas that of PUFA decreased gradually for 14 days under the same conditions. The highest SFA content was observed in the L-treated cells (32.33%) compared with that in the C- (26.08%), S- (23.15%), and LS-treated cells (27.60%), respectively, while the maximum MUFA content was identified in the S-treated cells (49.60%) compared with that in the C- (46.37%), L- (39.77%), and the LS-treated cells (43.91%). However, there was a slight difference in the PUFA content in the algal cells tested. The PUFA content in the C-, S-, L-, and the LS-treated cells was 27.54%, 27.72%, 27.88%, and 28.48%, respectively. Therefore, our findings indicated that algal *S. rubescens* KNUA042 cells have high SFA (C16:0) and MUFA (C16:1) contents and low PUFA (C18:3) content and can thus be a candidate for biodiesel production.

Table 1. Proximate and ultimate analysis of *S. rubescens* KNUA042 under different stress conditions at 0, 7, and 14 days.

	0 Day				7 Day				14 Day			
	C	S	L	LS	C	S	L	LS	C	S	L	LS
Proximate analysis (wt %)												
Moisture	6.6 ± 0.2	6.3 ± 0.1	6.5 ± 0.1	6.4 ± 0.1	6.6 ± 0.5	5.7 ± 0.1	7.0 ± 0.1	6.2 ± 0.0	5.1 ± 0.3	4.9 ± 0.2	5.7 ± 0.4	5.0 ± 0.3
Volatile matter	77.2 ± 0.4	75.5 ± 0.5	75.6 ± 0.4	75.9 ± 0.4	84.5 ± 0.3	87.5 ± 0.7	84.1 ± 0.4	85.8 ± 0.3	88.2 ± 0.1	90.5 ± 0.0	87.9 ± 0.4	89.2 ± 1.2
Ash	16.2 ± 0.2	18.2 ± 0.4	17.9 ± 0.6	17.7 ± 0.6	9.0 ± 0.2	6.8 ± 0.7	8.9 ± 0.4	8.0 ± 0.2	6.6 ± 0.2	4.6 ± 0.2	6.4 ± 0.8	5.8 ± 0.9
Ultimate analysis (wt %)												
Carbon (C)	42.2 ± 0.2	42.5 ± 0.4	42.7 ± 0.5	42.9 ± 0.3	48.0 ± 0.7	49.5 ± 0.3	47.4 ± 0.2	49.7 ± 0.2	54.1 ± 0.2	54.2 ± 0.1	53.1 ± 0.1	55.1 ± 0.4
Hydrogen (H)	6.4 ± 0.1	6.3 ± 0.1	6.4 ± 0.1	6.4 ± 0.1	7.3 ± 0.1	7.4 ± 0.0	7.2 ± 0.1	7.5 ± 0.0	8.2 ± 0.0	8.2 ± 0.0	8.1 ± 0.0	8.4 ± 0.1
Nitrogen (N)	6.6 ± 0.1	6.6 ± 0.0	6.6 ± 0.2	6.6 ± 0.0	4.2 ± 0.1	4.6 ± 0.0	4.1 ± 0.0	4.1 ± 0.0	3.0 ± 0.1	3.1 ± 0.0	3.2 ± 0.1	2.9 ± 0.0
Sulfur (S)	0.5 ± 0.0	0.5 ± 0.0	0.5 ± 0.0	0.5 ± 0.0	0.4 ± 0.0	0.4 ± 0.0	0.4 ± 0.0	0.4 ± 0.0	0.3 ± 0.0	0.3 ± 0.0	0.3 ± 0.0	0.3 ± 0.0
Oxygen (O) (by difference)	25.9 ± 0.2	25.9 ± 0.2	25.9 ± 0.2	25.9 ± 0.2	27.1 ± 0.1	28.7 ± 0.1	28.9 ± 0.0	25.9 ± 0.2	24.1 ± 0.5	24.7 ± 0.1	26.3 ± 0.4	25.2 ± 0.2
HHV (MJ/kg)	20.0 ± 0.0	20.1 ± 0.3	20.2 ± 0.2	20.2 ± 0.2	23.0 ± 0.4	23.5 ± 0.1	22.4 ± 0.2	24.0 ± 0.1	26.7 ± 0.2	26.7 ± 0.1	25.9 ± 0.0	27.2 ± 0.3

C, control (N deficiency); S, salinity (400 mM); L, high light intensity (1000 $\mu\text{mol m}^{-2} \text{s}^{-1}$); LS, combined stimulation (light intensity + salinity); HHV, higher heating value.

Table 2. Theoretical properties of a biodiesel produced from *S. rubescens* KNUA042 under different stress conditions at 0, 7, and 14 days according to ASTM and European standards.

	0 Day				7 Day				14 Day				EN 14214	ASTM D6751
	C	S	L	LS	C	S	L	LS	C	S	L	LS		
SV	162.2	164.3	161.4	162.4	183.8	188.6	188.5	191.8	188.8	191.3	191.7	194.1		
IV	164.4	165.6	163.1	164.5	118.9	124.5	112.1	108.4	103.6	106.6	102.2	105.3	≤120	
CN	33.4	33.5	33.5	33.4	50.0	49.6	51.7	53.4	54.4	54.1	54.7	54.4	≥51	≥47
DU	120	121	119	120	110	115	101	104	101	104	96	101		
CFPP	−10.2	−10.3	−10.2	−10.2	−5.7	−7.8	−4.3	−6.2	−5.4	−7.2	−3.6	−5.9	≤5/≤−20	
OS	5.6	5.6	5.6	5.6	7.2	7.3	7.0	7.7	8.6	8.8	7.7	8.2	≥6	≥3
ν	3.4	3.4	3.4	3.4	4.0	4.0	4.0	4.1	4.1	4.1	4.1	4.1	3.5–5.0	1.9–6.0
ρ	0.89	0.89	0.89	0.89	0.88	0.88	0.88	0.88	0.88	0.88	0.88	0.88	0.86–0.90	0.82–0.90

SV: Saponification value (mg KOH g^{-1}), IV: Iodine value ($\text{g I}_2 100 \text{g}^{-1} \text{fat}$), CN: Cetane number, DU: Degree of unsaturation, CFPP: Cold filter plugging point ($^{\circ}\text{C}$), OS: Oxidation stability (110 $^{\circ}\text{C}$ h), ν : Kinematic viscosity ($\text{mm}^2 \text{s}^{-1}$), ρ : Density (15 $^{\circ}\text{C}$) g cm^{-3} . C, control (N deficiency); S, salinity (400 mM); L, high light intensity (1000 $\mu\text{mol m}^{-2} \text{s}^{-1}$); LS, combined stimulation (light intensity + salinity).

3.8. Biodiesel Quality Assessment

Given that fatty acid composition varied by N-deficiency-dependent high salinity, high light intensity, and combined light intensity and salinity, the theoretical fuel properties of the biodiesel quality were estimated using the ASTM and EN standard for biodiesel production. Table 2 shows the key criteria for estimating the biodiesel parameters, including the SV, CN, iodine value (IV), DU, CFPP, kinematic viscosity (ν), density (ρ), and OS. The theoretical properties of the algal biodiesel were found to be within the ASTM D6751 (USA) and EN 14214 (European Unit) standards, and no differences were found in the biodiesel quality parameters. The quality properties of the biodiesel in the algal biomass exposed to abiotic stress for 14 days were low density (ρ ; 0.88 g cm^{-3}), low kinematic viscosity (ν ; $4.1 \text{ mm}^2 \text{ s}^{-1}$), high CN (54.1–54.7), high OS (7.7–8.8 h), CFPP ($-7.2 \text{ }^\circ\text{C}$ – $-3.6 \text{ }^\circ\text{C}$) and IV (102.2 – $106.6 \text{ g I}_2 (100 \text{ g})^{-1} \text{ fat}$). Additionally, the values of SV and DU were 188.8 – $194.1 \text{ mg KOH g}^{-1}$ and 96 – 104 , respectively, in all the C-, S-, L- and LS-treated algal cells (Table 2); the initial values for all the C-, S-, L-, and LS-treated algal cells tested were adjusted to 161.4 – $164.3 \text{ mg KOH g}^{-1}$ of SV, 163.1 – $165.6 \text{ [g I}_2 (100 \text{ g})^{-1} \text{ fat]}$ of IV, 33.4 – 33.5 of CN, 119 – 121 of DU, $-10.2 \text{ }^\circ\text{C}$ – $-10.3 \text{ }^\circ\text{C}$ of CFPP, 5.6 h of OS, $3.4 \text{ mm}^2 \text{ s}^{-1}$ of ν , and 0.89 g cm^{-3} of ρ . Taken together, our results indicated that the microalgal oil extracted from *S. rubescens* KNUA042, especially the stressed cells, would transfer to biodiesel in the form of lower emissions, good combustion, good cold flow properties at low temperatures, and an excellent OS.

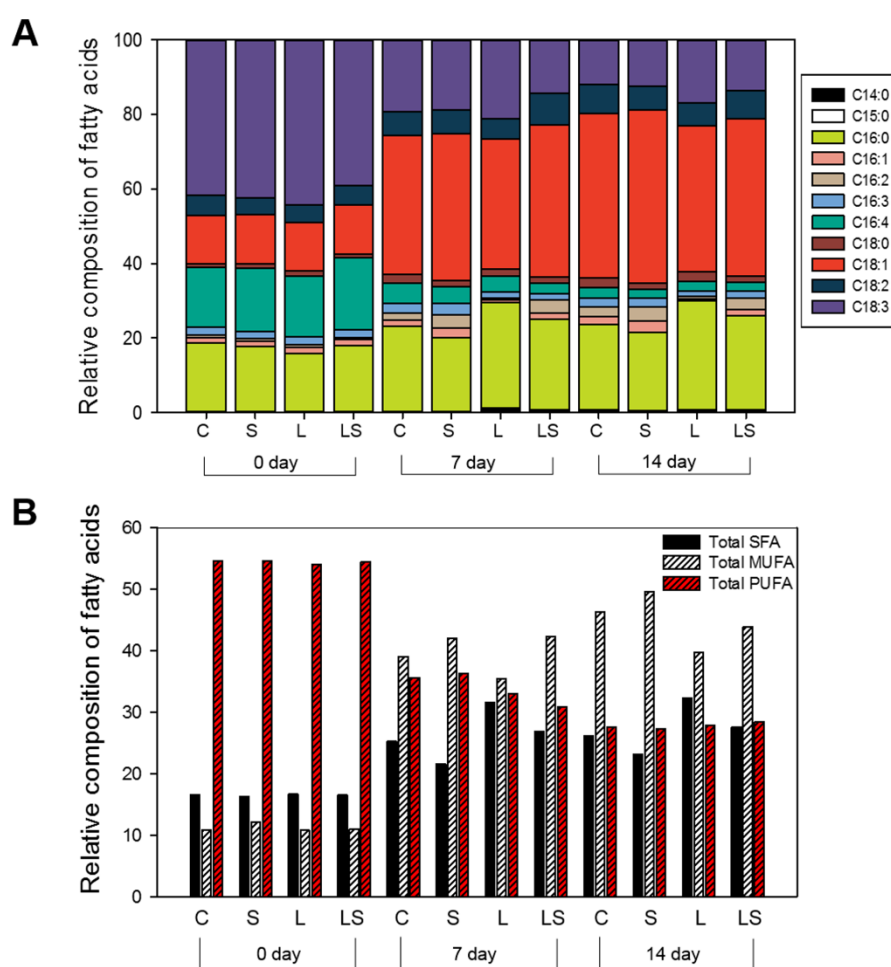


Figure 4. Fatty acid profiles of *S. rubescens* KNUA042 under different stress conditions at 0, 7, and 14 days. (A) Relative composition of total fatty acids; (B) relative composition of saturated (SFA), monounsaturated (MUFA), and polyunsaturated fatty acids (PUFA). C, control (N deficiency); S, salinity (400 mM); L, high light intensity ($1000 \mu\text{mol m}^{-2} \text{ s}^{-1}$); LS, combined stimulation (light intensity + salinity).

3.9. Pigment Analysis

Total carotenoid content was examined under salinity, light intensity, and combined salinity and light intensity in the presence of N deficiency. In the phenotype-based analysis, LS-treated algal cells resulted in a complete color shift from green to orange after 14 days of stress treatment. In terms of color intensity, the L-treated algal cells exhibited a mild color change, but it was less intense than that exhibited by the LS-treated cells. The C- and S-treated algal cells slightly faded from green under the same culture conditions (Figure 5A and Figure S7). *S. rubescens* KNUA042 cells were healthy during the cultivation periods, although there was a difference in each cell condition between the stressors (Figure 5B). However, the *S. obliquus* KNUA017 and KNUA025 cells that were used as reference exhibited a relatively poor survival rate under the same conditions as the KNUA042 cells (Figure S8A–C, lower panel). These results suggested that *S. rubescens* KNUA042 has a better intrinsic stress tolerance compared with other *Scenedesmus* sp. and that the algal strain has other promising biochemical characteristics such as those involving metabolites.

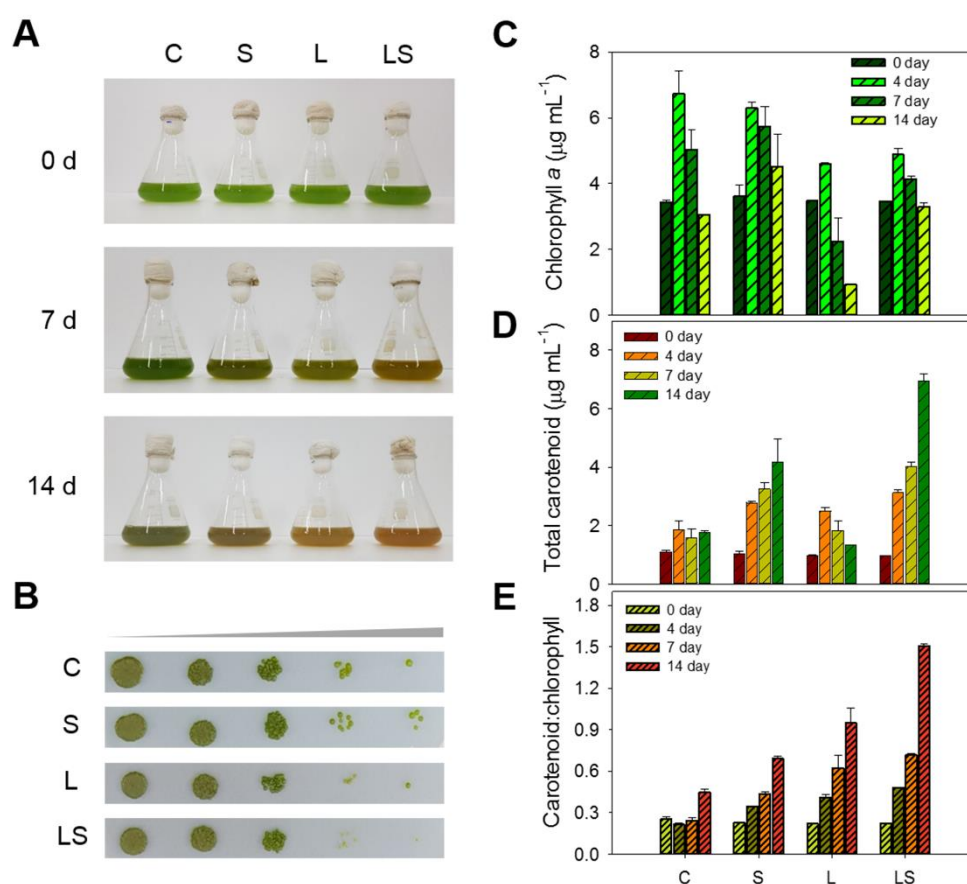


Figure 5. (A) Changes in culture color of *S. rubescens* KNUA042 cells during culture under stress conditions at 0, 7, and 14 days. (B) Spotting assay on BG-11 solid cultivation of *S. rubescens* KNUA042 after stress treatment from 14 days. Time course of chlorophyll *a* content (C), total carotenoid content (D), and carotenoid/chlorophyll ratio (E) under different stress conditions. C, control (N deficiency); S, salinity (400 mM); L, high light intensity ($1000 \mu\text{mol m}^{-2} \text{s}^{-1}$); LS, combined stimulation (light intensity + salinity).

Total chlorophyll *a* and carotenoid contents were analyzed in the algal cells exposed to abiotic stress treatments. The initial total chlorophyll *a* content in the algal cells was approximately 3.44 ± 0.05 – $3.60 \pm 0.34 \text{ mg L}^{-1}$. Over the first 4 days of the experiment, the chlorophyll *a* content in stressed cells increased to 4.59 ± 0.04 – $6.73 \pm 0.68 \text{ mg L}^{-1}$ but then decreased gradually to 0.92 – $4.52 \pm 0.97 \text{ mg L}^{-1}$ over the remaining days of the trial. Following the 14-day stress treatment, the highest chlorophyll *a* content was $4.52 \pm 0.97 \text{ mg L}^{-1}$ recorded in the S-treated cells, while the lowest chlorophyll *a* content

was 0.92 mg L^{-1} recorded in the L-treated cells. In the C- and LS-treated algal cells, chlorophyll *a* contents were 3.05 ± 0.01 and $3.29 \pm 0.11 \text{ mg L}^{-1}$, respectively (Figure 5C). Next, the total carotenoid content increased over time under the same conditions. The starting value for the algal cells was 0.97 ± 0.01 – $1.01 \pm 0.05 \text{ mg L}^{-1}$ and then the values after C, S, L, and LS treatment for 14 days were 1.75 ± 0.06 , 4.15 ± 0.82 , 1.32 ± 0.02 , and $6.94 \pm 0.06 \text{ mg L}^{-1}$, respectively. During stress exposure, the highest value was observed in the LS-treated cells ($6.94 \pm 0.06 \text{ mg L}^{-1}$), whereas the lowest value was detected in the L-treated cells ($1.32 \pm 0.02 \text{ mg L}^{-1}$). Although the concentration in L-treated cells was lower than that in the other algal cells, the maximum value was identified at $2.49 \pm 0.12 \text{ mg L}^{-1}$ in the L-treated cells for 14 days (Figure 5D). As a result, the ratio of carotenoids to chlorophyll was augmented in a time-dependent manner and maximized to the stressed algal cells for 14 days. The best ratio was 1.50 ± 0.01 , identified in the LS-treated cells, whereas the minimum ratio was 0.39 ± 0.04 identified for the C-treated cells. The ratio of the S- and L-treated cells was 0.69 ± 0.01 and 0.94 ± 0.01 , respectively (Figure 5E). Our results showed that *S. rubescens* KNUA042 was capable of producing bioactive pigment compounds, of which two were particularly promising: chlorophyll and carotenoids.

To quantify how the pigment content changed by N deficiency-dependent salinity and high light intensity, crude pigment extracts of algal cells were exposed to stress for 14 days and examined using HPLC. Among the identified pigments, the major compounds were chlorophyll *a*, astaxanthin, canthaxanthin, and lutein. As shown in Figure 6, lutein and chlorophyll *a* content decreased in a time-dependent manner under all stress conditions. The initial concentration of chlorophyll *a* in unstressed algal cells was 12.03 ± 0.38 – $15.22 \pm 0.68 \text{ mg g}^{-1}$, whereas the final (14 day culture) concentrations in the C-, S-, L-, and LS-treated algal cells decreased to 4.34 ± 0.72 , 4.28 ± 0.26 , 1.13 ± 0.05 , and $3.68 \pm 0.01 \text{ mg g}^{-1}$, respectively. Among these treatments, the lowest value was observed in the L-treated algal cells (Figure 6A). The lutein content in the algal cells were adjusted to 2.09 ± 0.01 – $2.59 \pm 0.33 \text{ mg g}^{-1}$ of the starting concentration and was decreased to 0.79 – $1.98 \pm 0.29 \text{ mg g}^{-1}$ under stress conditions for 14 days. The lowest concentration ($0.79 \pm 0.01 \text{ mg g}^{-1}$) was also observed in the L-treated cells and the highest concentration ($1.98 \pm 0.29 \text{ mg g}^{-1}$) was detected in the S-treated cells; the concentration in the C- and LS-treated cells was 1.36 and $1.76 \pm 0.08 \text{ mg g}^{-1}$, respectively (Figure 6B).

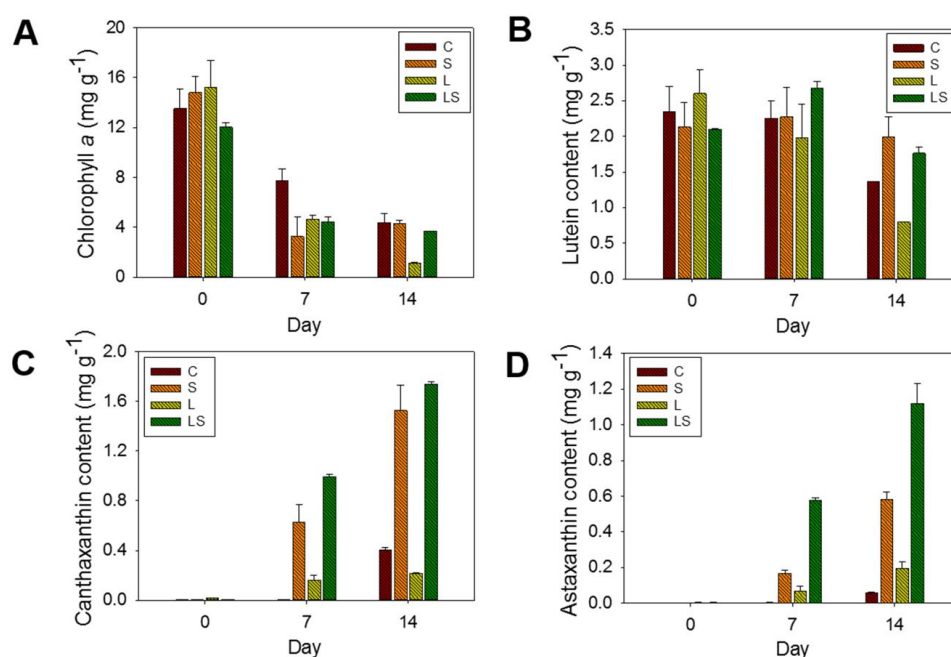


Figure 6. Pigment contents of (A) chlorophyll *a*, (B) lutein, (C) canthaxanthin, and (D) astaxanthin in the culture of *S. rubescens* under stress conditions at 0, 7, and 14 days, as determined by HPLC. C, control (N deficiency); S, salinity (400 mM); L, high light intensity ($1000 \mu\text{mol m}^{-2} \text{s}^{-1}$); LS, combined stimulation (light intensity + salinity).

Regarding the secondary carotenoids, the concentrations of canthaxanthin and astaxanthin were also quantified in the stress-treated algal cells. While canthaxanthin was not detected in unstressed cells, its concentration in stressed algal cells was 0.21 ± 0.01 – 1.73 ± 0.01 mg g⁻¹. In the C-treated cells, canthaxanthin was only recorded in the algal biomass exposed to N deficiency for the full 14 days, and its concentration was 0.40 ± 0.01 mg g⁻¹. Concentrations increased gradually with time, from 0 mg g⁻¹ in the S-, L-, and LS-untreated algal cells at 0 days to 1.52 ± 0.20 , 0.21 ± 0.01 , and 1.73 ± 0.01 mg g⁻¹ in the S-, L-, and LS-treated cells at 14 days, respectively (Figure 6C). At 14 days, the LS-treated algal cells had the highest molecular concentration of canthaxanthin, which was 4.32-fold, 1.13-fold, and 8.23-fold greater than that in the C-, S-, and L-treated cells, respectively. In addition to canthaxanthin concentration, the astaxanthin concentration was also measured under the same conditions. The pattern of astaxanthin accumulation was similar to that of canthaxanthin. The astaxanthin molecule had not been identified in the unstressed algal cells for 0 days; however, astaxanthin had accumulated in a time-dependent manner in the stressed algal cells, except for the N-deficient cells. Astaxanthin was detected in the N-deficient cells following stress treatment for 14 days at 0.05 mg g⁻¹. Conversely, the astaxanthin content in the S-, L-, and LS-treated algal cells after 14 days was increased by 0.58 ± 0.01 , 0.19 ± 0.04 , and 1.11 ± 0.11 mg g⁻¹, respectively. The astaxanthin content in the LS-treated algal cells showed that the highlighted value (1.11 ± 0.11 mg g⁻¹) was 22.20-fold, 1.91-fold, and 5.84-fold higher than that in the C-, S-, and L-treated algal cells, respectively (Figure 6D). Overall, the concentrations of canthaxanthin and astaxanthin were in the order of the LS-, S-, C-, and L-treated algal cells. Hence, as shown in our results, the TSC system transferring from the N-abundant conditions to the N-deficient conditions was introduced in the presence of high light intensity to enhance biomass and carotenoid production. These trials could be a vital consideration toward building a future cultivation operation.

4. Discussion

4.1. Morphological and Molecular Characteristics of *S. rubescens* KNUA042

Preliminary morphological analysis showed that the KNUA042 cells were nonmotile, with a round and slightly ellipsoid shape and diameters of 6 to 10 μm. Cytological analysis revealed that the algal KNUA042 cells possessed a chloroplast containing one pyrenoid that was divided into two cells at the vegetative stage (Figure S1C). In phylogenetic tree analysis using ITS2 and 18S rRNA, KNUA042 was shown to belong to a member of *Scenedesmus* sp. (Figure S2) and to *S. rubescens* (Figure S3). Ultimately, the 18S rRNA sequence confirmed that the highest sequence relatedness was found with the green algae *S. rubescens*.

Currently, there are approximately 74 taxonomically accepted species of *Scenedesmus*, of which the three major groups are *Acutodesmus*, *Desmodesmus*, and *Scenedesmus* [36]. *Acutodesmus* is characterized as having acute cell poles, whereas *Desmodesmus* and *Scenedesmus* have obtuse or truncated cell poles [36]. Furthermore, *Scenedesmus* could be divided into two subgenera—the non-spiny *Scenedesmus* and the spiny *Desmodesmus*. *Scenedesmus* either exist as unicells or as coenobia comprising four or eight cells inside a parental mother wall. Various coenobial architectures have been reported, including linear, costulatoid, irregular, alternating, or datylococcoid patterns [36]. Considering what all of the results revealed in terms of morphology, such as the coenobia and multiple nucleotide sequences, our results suggested that this algal strain was related to *S. rubescens* and was thus termed *S. rubescens* KNUA042.

4.2. Nutrient Consumption of *S. rubescens* KNUA042

The optical density data showed a striking difference, with the highest absorbance values being recorded for the 50 mg L⁻¹-treated algal cells (Figure S4). According to previous reports, of *S. rubescens*-like microalgae, algae grown in BG-11 medium and treated with 7–10 mM NaNO₃ produced the highest biomass content compared to that observed with other treatments [37]. In the case of *D. salina*, growth and biomass productivity were directly related to the N levels, with the highest biomass concentrations shown to occur under 0.05 mM or 5 mM N regimes, 495 mg L⁻¹

and 1409 mg L⁻¹, respectively [38]. Similarly, our results indicated that the algal KNUA042 cells demonstrated optimal growth when the cells were subjected to approximately 50 mg L⁻¹ NaNO₃. In a study of batch cultures of green and blue-green algae, elevated N levels led to an increase in biomass, protein, and chlorophyll contents, whereas lower N levels resulted in the accumulation of total lipids, especially neutral lipids such as TAGs [39]. Thus, to manipulate mass culture to yield biomass with the desired products, including different lipid-derived compounds such as carotenoids, subsequent experiments were performed with an NaNO₃ of 25 mg L⁻¹ rather than that of 50 mg L⁻¹.

For algal KNUA042 cells grown in BG-11 medium treated with 25 mg L⁻¹ NaNO₃, growth kinetics, N consumption, and dry weight were all shown to increase over time during the culture periods (Figure 1). Under these conditions, most of the N was consumed by the 14th day of culturing, at which point the optical density and dry weight were 0.939 and 0.35 g L⁻¹, respectively. For algal cells grown in BG-11 medium supplemented with 50 and 250 mg L⁻¹, the remaining concentration of NaNO₃ was 5.66 and 125.64 mg L⁻¹, respectively, at the end of the same culture period (Figure S4A). Essential inorganic nutrients such as N and P have critical effects on the growth, reproduction and metabolism of microalgae. Nutrient limitation is an applied and remarkable strategy used to change and regulate the algal cell cycle and its physiological response is related to the metabolism of lipids and their by-products, such as carotenoids [40]. Nutrient deficiency induced undesirable performance in the algal cells but promoted lipid production. When algal cells were subjected to N stress conditions, the microalgae steadily decreased their rate of cell division and their active biosynthesis of desired products. The effects of N limitation on different algal strains used to explore and optimize various output parameters have been demonstrated in many studies. In particular, N starvation triggered lipid accumulation, especially TAGs, in microalgae such as *Scenedesmus* sp. [40–44]. In general, an inverse relationship has been reported between lipid and nutrient concentrations [43].

4.3. Lipid and Biomass Productivity under Abiotic Stress in the Presence of N Deficiency

In general, lipids in the microalgae were highly accumulated by applying stressors such as N depletion, light intensity, temperature, high salinity, and heavy metals [45]. Based on these facts, lipid content and biomass productivity were estimated when the algal KNU042 cells were exposed to abiotic stress in the presence of N deficiency. As shown in Figure 2, dry weight increased in a time-dependent manner during the additional culture periods, which corresponded to the lipid content and lipid productivity. The lipid content and dry weight were the highest in the LS-stressed cells compared to those in the single stress-treated cells (Figure 2A,B). In the C- or L-treated cells, there was no difference in biomass and lipid productivity, and the productivity values of these cells were lower than those of S- and LS-treated cells (Figure 2C). In *S. rubescens* KNUA042, high light intensity (1000 μmol m⁻² s⁻¹; L) appeared to induce cellular damage, whereas salinity stress (400 mM NaCl; S) caused an adaptive response to the unfavorable conditions via the activation of an array of cell rescue systems because the dry weight and biomass productivity of the S-treated algal cells increased 1.2-fold than those of the C- and L-treated cells. Accordingly, LS-treated algal cells enhanced the acquired tolerance by minimizing cellular damage via a salt-mediated gene expression program, which led to the highest productivity of lipids and biomass.

Recent research has shown that numerous algal species produce and accumulate lipids, particularly TAG, under N-limited mixotrophic conditions [40]. However, our results suggest that N-limited autotrophic conditions, coupled with elevated salinity and light intensity, could have a positive effect on the biosynthesis of desired output products by controlling the biochemical pathways in the algal KNU042 cells. Firstly, under N-limited conditions (C) alone, the lipid content of the *S. rubescens* KNUA042 cells was 38.14% ± 0.82%, whereas a previous study has demonstrated that *Chlorella* sp. cells grown in N-deficient medium exhibited a maximum lipid content of 36.7% [46]. These results are similar to the maximum yield of 41% obtained for *Scenedesmus* sp. SP-1 grown in culture media supplemented with 130 mg L⁻¹ NaNO₃ [47]. The lipid content in the *S. rubescens* KNUA042 cells in

our study was higher than the moderate lipid content of 10%–39% obtained from other *Scenedesmus* species [48].

Secondly, salt stress has been known to cause osmotic pressure within the algal cells, generating a stress response that modifies their metabolism and causes accumulation of lipids and antioxidants (β -carotene and astaxanthin) and reduction of biomass [49,50]. As a result, microalgae adapted to these new conditions significantly increase their total lipid content, as well as their lipid composition [40]. The lipid content in the *S. rubescens* KNUA042 cells challenged with 400 mM NaCl was $38.47\% \pm 0.88\%$. Experiments with *Chlamydomonas mexicana* and *S. obliquus* grown in culture media with a range of different supplemental salt concentrations have shown that 25 mM NaCl produced maximum lipid content (37% and 34%, respectively) [51]. *C. vulgaris* and *A. obliquus* also produced their maximum lipid contents (49% and 43%, respectively) when the cells were treated with 400 mM NaCl [45]. Although results regarding the effects of NaCl on microalgae are scarce and conflicting, our results showed that higher salinity could improve the lipid production of *S. rubescens* KNUA042 cells.

Thirdly, light intensity is one of the most important parameters determining the development of microalgae and their production of biomass and lipids [40]. Biomass productivity and lipid content of *S. rubescens* KNUA042 cells were $60.71 \pm 0.01 \text{ mg L}^{-1} \text{ d}^{-1}$ and $20.21 \pm 0.18 \text{ mg L}^{-1} \text{ d}^{-1}$, respectively, under the high light intensity condition ($1000 \mu\text{mol m}^{-2} \text{ s}^{-1}$). Extremely high light intensity causes unfavorable growth and stress responses such as photoinhibition and photooxidation in algal cells. These conditions affect the lipid content negatively by causing lipid peroxidation [40]. In order to mitigate these unfavorable conditions, the algal cells accumulate neutral lipids and antioxidants (β -carotene and astaxanthin), while reducing polar lipids and biomass [52]. *S. rubescens* KNUA042 cells exposed to elevated light intensity treatment (L) of $1000 \mu\text{mol m}^{-2} \text{ s}^{-1}$ showed decreased lipid content compared with the C- and S-treated cells. Identifying the optimum range of light intensity means that creating a higher lipid production for this strain is therefore an important priority, but this has yet to be elucidated.

Finally, a combination of L+S was trialed, and the maximum productivity of biomass ($80.71 \pm 4.04 \text{ mg L}^{-1} \text{ d}^{-1}$) and lipids ($34.75 \pm 1.64 \text{ mg L}^{-1} \text{ d}^{-1}$) as well as the maximum lipid content ($42.99 \pm 0.72\%$) were shown to have increased by up to 30.64%, 71.94%, and 27.87%, respectively, compared to the results for either of these treatments alone. In addition, in comparison to the combined effects of N limitation ($130 \text{ mg L}^{-1} \text{ NaNO}_3$), high salinity (343 mM NaCl), and high light intensity ($200 \mu\text{mol m}^{-2} \text{ s}^{-1}$) on *Scenedesmus* sp. in a similar study, lipid productivity and lipid content of *S. rubescens* KNUA042 cells in the present study were higher [47]. Similarly, in *H. pluvialis*, combinations of three stress factors (high light intensity + salinity, high light intensity + iron, or salinity + iron) also produced a sustained increase in by-products. Moreover, another study found that the highest production of biomass was obtained when all the three factors (high light intensity, salt, and iron) were applied simultaneously [53]. Taken together, these results showed the possibility of accelerating the maximum lipid productivity by providing a combination of physico-chemical stresses (salinity + light intensity) coupled to N deficiency in *S. rubescens* KNUA042 cells.

4.4. Lipid Accumulation as a Biofuel Feedstock

As shown in Figure 3, BODIPY dyes were very effective in determining the fluorescence intensity of the S- and LS-treated algal cells. While Nile red displayed a lower fluorescence with higher salinity, which suggested a shift in the peak emission and retardation of the dye transfer into the lipid droplets. Thus, this result provided a limitation to determining Nile red fluorescence under hypersaline conditions [54]. Salt stress seemed to accelerate high accumulation of lipid content by increasing the cell size and cell mass of *S. rubescens* KNUA042 cells (Figure 3); however, this phenomenon was not observed under light stress. Some studies have shown that salt-stressed microalgae caused morphological changes such as cytoplasmic vacuolization, extreme deformation of the mitochondria, and ultrastructural changes in the Golgi and ER [55]. For instance, the algal *Parachlorella kessleri* cells, when exposed to salt stress, increased in cell size and lipid droplet content [56]. Thus, our

results indicated that high salinity accelerated the cell weight and lipid accumulation, whereas light intensity reduced cell mass and lipid droplets. Furthermore, a combination of salinity and high light intensity generated the highest cell weight and fluorescence intensity via operating a synergistic biochemical pathway rather than a single stress response.

The highest signal intensity for TAG content was observed in the 14-day S-treated algal cells, whereas the lowest intensity was detected in the L-treated algal cells (Figure S6B). During the process of photosynthesis and stress response, nonpolar lipid TAG is stored in microalgae cells, playing a fundamental role in energy storage [57]. Thus, TAG is considered a valuable by-product due to its important commercial value [40,58]. The results of the present study support the idea that the accumulation of TAGs can be influenced under specific conditions such as nutrient starvation or high-stress environments [40]. In addition, to its function in energy storage, the TAG produced in this way could be used to conduct other biological activities [59]. Thus, our results show that the production of TAG in algal *S. rubescens* KNUA042 cells can be increased at different environmental stress levels and suggested that this is important for energy storage against abiotic stress too, since the accumulated TAG could be used to construct cellular membranes or to produce the cell rescue biomolecules.

4.5. Proximate and Ultimate Analysis

When the algal cells were challenged to a specific stress for 14 days, the moisture content gradually decreased in a time-dependent manner; the values were 5.1 ± 0.3 , 4.9 ± 0.2 , 5.7 ± 0.4 , and 5.0 ± 0.3 wt%, respectively, in the C-, S-, L-, and LS-treated cells. In particular, the moisture content of the S- and LS-treated algal cells was <5 wt% (Table 1). Low moisture content was important for the preservation of nutritional integrity, because the presence of lipid water could increase the microbial activity and deterioration of the food products [60]. In this regard, our results suggested that the by-products of the S- and LS-treated algal cells could have a potential application in the food industry based on moisture alone, whereas the biomass of the C- and L-treated cells might be effective for biodiesel production.

The ash content of all algal cells decreased from 16.2 ± 0.2 – 18.2 ± 0.4 wt% at day 0 to 4.6 ± 0.2 – 6.6 ± 0.2 wt% under the stress conditions at 14 days, with the largest decline observed in the S-treated cells (Table 1). Generally, lower ash content has been found in green microalgae (14.3 ± 0.1 wt%) [61]. In contrast, volatile matter increased from 75.5 ± 0.5 – 77.2 ± 0.4 wt% at the start of the experiment to 87.9 ± 0.4 – 90.5 ± 0.0 wt% in the C-, S-, L-, and LS-treated cells at 14 days (Table 1). Among the microalgal groups, green microalgae have been shown to be composed of more volatile matter than brown microalgae, as the latter possess a much greater ash content (43.4 ± 0.2 wt%) [62]. For example, volatile matter content in *Spirulina platensis*, *C. vulgaris*, and *Nannochloropsis oculata* has been recorded at 82.3 wt%, 84.3 wt%, and 67.45 wt%, respectively [62]. Reportedly, a high volatile matter content ($>80\%$) in microalgal biomass is advantageous for biofuel production [33]. Given that the proximate analysis of *S. rubescens* KNUA042 indicated that it is characterized by low moisture content, high volatile matter, and moderate ash content, the study supports its potential as a biomass fuel. Table 1 shows the C, H, N, and O proportion of ash biomass from the unstressed and stressed algal cells.

No differences were found in any of the measured content values of algal cells prior to stress exposure; however, the values changed in a time-dependent manner during the 14-day stress treatment, although a promising difference was not observed in all of the algal cells tested (C-, S-, L-, and LS-treated cells). Following the stress treatments at 14-days, C and H content was about 54.12 and 8.22 wt%, respectively. In addition, HHV, as calculated based on Given's equation for microalgal biomass was 20.1 MJ kg^{-1} calories before stress treatment, which is higher than the cellulosic biomass of approximately 18.6 MJ kg^{-1} [63]. On the 14th day of stress treatment, LS biomass had the highest calorific value (27.2 MJ kg^{-1}), which is approximately 36% higher than that of the untreated microalgae biomass (approximately 20 MJ kg^{-1}) (Table 1). Considering the high content of C and H, the algae could be an advantageous as a feedstock in biofuel production [33]. The results of the present study

clearly showed that the stressed algal *S. rubescens* KNUA042 cells showed potential for use in biodiesel production, especially the LS-treated cells.

4.6. Fatty acid Profiling

The results of the present study show that the fatty acids C16:0, C18:1, and C18:3 were potentially suitable for biodiesel production (Figure 4), as reported previously [64]. Among these, C18:1 is an important indicator of biodiesel quality and provides great stability [65]. Another study has shown that C18:1 content increases at the expense of C16:0 or C18:3 under N starvation conditions in *Parietochloris incisae* [66] and *S. rubescens*-like microalgae [67]. Following the 14-day stress treatment in the present study, the C16:4 and C18:3 content in the algal cells had decreased on average by 2.52% and 13.89%, respectively (Figure 4). According to the EN standard for biodiesel (EN 14214), the proportion of linolenic acid (C18:3) should not be >12% [68]. Assessments of the fatty acids in crude oil extracts from microalgae indicate that the content of fatty acid (C16:4) in the present algal strain, those with ≥ 4 double bonds, make it a good source stock for biodiesel production [68].

Abiotic stress treatments (L, S, and LS) resulted in high accumulations of both SFA and MUFA, whereas the level of PUFA decreased in the algal KNU042 cells following accumulation of neutral lipids, such as C18:3n3 (Figure 4). The accumulation of SFA and MUFA coupled with the reduction of PUFA, has been previously reported under high L and S stress [69]. For instance, *C. zofingiensis* accumulated a large amount of C18:1 under high light conditions, while the level of PUFA C16:3 declined by approximately 50% [70]. Similarly, in *Scenedesmus obtusus*, the concentration of C18:1 was shown to increase from 17.8% to 39.4% under high salinity conditions [71]. In agreement with the results of the current study, low light intensity is known to increase PUFA content; while high light intensity results in a greater accumulation of SFA and MUFA [72]. Work on the *Monoraphidium* sp. also supports the current findings, since a combination of temperature and high light intensity was found to benefit lipid production, especially of the desired neutral lipids such as TAG and the fatty acids C16:0 and C18:1, which were further promoted under combined stress conditions [73]. Therefore, our findings, which show that algal *S. rubescens* KNUA042 cells are high in SFA (C16:0) and MUFA (C16:1) but low in PUFA (C18:3), suggest that this strain is a candidate for biodiesel production.

4.7. Biodiesel Quality Estimation as a Biofuel Feedstock

Although most of the parameters matched ASTM D6751 and the EN 14214 standard, the values of SV, CN, CFPP OS, and ν in the algal cells increased under C-, S-, L-, and the LS-treated conditions, whereas the values of IV decreased under the same conditions. Specifically, the CN parameter, which is the main indicator of diesel fuel combustibility, was satisfied via the algal cells exposed to abiotic stress for 7 days (49.6–53.4) or more (54.1–54.7); however, this was not the case for the unstressed cells (Table 2). In the estimated properties for algal biodiesel, SV, IV, CN, DU, and the CFPP value of *Scenedesmus* spp. was 152.99 mg KOH g⁻¹, 99.57 (g I₂ (100 g)⁻¹ fat), 59.57, 86.86, and -6.91 °C, respectively [74]. Except for CN, all values for *S. rubescens* KNUA042 analyzed were similar to those of *Scenedesmus* sp. There was a direct relationship between the DU and the CN, IV, SV, CFPP, CN, SV, and the length of the fatty acid chains. In other words, the higher the length of the fatty acid chains, the larger the CN and SV will be [74]. In addition, the higher the DU and polyunsaturation, the larger the IV, and the lower the CFPP values will be. *S. rubescens* KNUA042 cells displayed the lowest PUFA under stressed conditions, compared to the unstressed cells. Such a fatty acid profile resulted in a lower DU value (Table 2). The SFA, MUFA, and PUFA contents of the stressed algal cells were 27.29 ± 3.83%, 44.91 ± 4.14%, and 27.88 ± 0.53%, respectively (Figure 4). The general standards used for biodiesel production prefer crude oil extract with a high proportion of SFAs and MUFAs, since these fatty acids were important for increasing the energy yield and providing the superior oxidative stability of biodiesel. Taken together, our results indicated that the microalgal oil extracted from the *S. rubescens* KNUA042, especially the stressed cells, would transfer to biodiesel in the form of lower emissions, good combustion, good cold flow properties at low temperatures, and an excellent OS.

4.8. Pigment Analysis

Under stress conditions, *S. rubescens* KNUA042 cells exhibited highly elevated SFA (C16:0) and MUFA (C18:1) content, whereas PUFA, such as C16:4 and C18:3 belonging to polar lipids, content was decreased (Figure 4). Increases in and accumulation of the neutral lipids C16:0 and C18:1 are closely related to secondary metabolite production [69]. Based on these results, total carotenoid content was examined under N-deficiency-dependent salinity and high light intensity. The total concentration of chlorophyll *a* decreased gradually to $0.92\text{--}4.52 \pm 0.97 \text{ mg L}^{-1}$ in the stressed algal cells (C, S, L, and LS) during the cultivation periods (Figures 5C and 6A), whereas the total carotenoid content increased with time under the same conditions. (Figure 5D). As a result, the ratio of carotenoids/chlorophyll was augmented in a time-dependent manner and peaked in the stressed algal cells at 14 days. Among the 14-day ratios, the best value was 1.50 ± 0.01 observed in the LS-treated cells, whereas the minimum ratio was 0.39 ± 0.04 recorded in the C-treated cells. The ratios in the S- and L-treated cells were 0.69 ± 0.01 and 0.94 ± 0.01 , respectively (Figure 5E). The carotenoid/chlorophyll ratio is a stress indicator and can show that lipid synthesis has been induced, and in the case of an augmented ratio, it can also be a marker of physiological stress in microalga under poor environmental conditions [66,75]. Our results showed that *S. rubescens* KNUA042 was capable of producing bioactive pigment compounds, two of which were particularly promising chlorophyll and carotenoids.

Among the identified pigments, the major compounds were astaxanthin, canthaxanthin, and lutein. Lutein content in stressed algal cells decreased over time from $2.09 \pm 0.01\text{--}2.59 \pm 0.33 \text{ mg g}^{-1}$ to $0.79\text{--}1.98 \pm 0.29 \text{ mg g}^{-1}$. The lowest value was observed in the L-treated cells, while the highest was detected in the S-treated cells (Figure 6B). Currently, temperature is the only factor known to enhance the production of lutein, while even the temperature effect on carotenoid production is not well-established [72]. Our results showed that high salinity enhances the biosynthesis of lutein under N-limited condition and that high light intensity coupled with high salinity can enhance the metabolic pathway of these compounds. This benefit of combined stresses was clearly observed in the contrasting concentrations of lutein in the L-treated algal cells, which had the lowest value among the stress treatments.

The concentrations of canthaxanthin and astaxanthin increased gradually with time during the culture periods. Canthaxanthin was not detected in the unstressed cells but increased in concentration to $0.21 \pm 0.01\text{--}1.73 \pm 0.01 \text{ mg g}^{-1}$ in the stressed algal cells. The molecular concentration of canthaxanthin reached its highest value in the LS-treated algal cells compared with that observed in the C-, S-, and L-treated cells (Figure 6C). The pattern of astaxanthin accumulation was similar to that of canthaxanthin. The astaxanthin molecule was not identified in the unstressed algal cells at 0 days; however, it accumulated in a time-dependent manner in the stressed algal cells, with the exception of the N-limited cells. The maximum astaxanthin content was reached in LS-treated algal cells (Figure 6D). Overall, concentrations of canthaxanthin and astaxanthin, from highest to lowest, were recorded in the LS-, S-, C-, and the L-treated algal cells. Microalgae can generate high production levels of carotenoids when under conditions of stress, including high salinity, high light intensity, or nutrient limitation such as N [45]. The absence or low levels of N activate rapid and effective physiological responses, which further enhance secondary biosynthetic pathways in the green algae [72]. Hence, as shown in our results, the TSC system that transfers cultivation from an initial N-abundant condition to an N-deficient condition introduced in the presence of high light intensity, is capable of enhancing biomass and carotenoid production. These trials may be a vital step toward building future cultivation operations.

As shown in Figure 6, high salinity is likely the most successful at inducing overproduction of carotenoids (β -carotene and astaxanthin) and lutein in a number of species; however, the effect of salinity on carotenoid production is complex [72]. Similar to salinity, high light intensity is an environmental factor that greatly affects microalgal metabolism, including photosynthesis, cell composition, and metabolic pathways, and these conditions affect the economic efficiency of the algae cultivation process [76]. In most algal species, high light intensity enhances the concentration of astaxanthin and lutein [72]. However, unlike that observed in other microalgae, high light intensity produced only

a moderate accumulation of lutein, canthaxanthin, and astaxanthin in algal cells of the *S. rubescens* KNUA042 cultured for 14 days. Compared with that observed for the other stress treatments, these were among the lowest levels (Figure 6). Excess light intensity is known as an important factor in ROS production in microalgae, causing both photoinhibition and photooxidation [72]. Thus, a high accumulation of ROS usually influences cell growth in an adverse way, with the additional effects decreasing the yield of desired products and total biomass [52]. Conversely, a combination of unfavorable stress factors might result in enhanced accumulation of carotenoids from the algal biomass. These results may be, at least partially, explained by the TSC concept. Cultivation of the algal strain *S. rubescens* KNUA042 under a combination of high salinity and N deficiency conditions could further enhance the production of carotenoids such as astaxanthin, canthaxanthin, and lutein relative to TSC cultivation under single stress (only N deficiency) (Figure 6). In *Scenedesmus* sp., the combination of N-deficiency-dependent light intensity and high salinity seems to increase the production of astaxanthin and canthaxanthin [47]. Coupling several environmental stresses in a single culture condition could become a novel strategy for improving high-value metabolite production; however, the dependency of metabolic pathways on stress type in various algal strains is a complicated development and one that is not yet well-understood [72].

Taken together, our results suggested that an N-deficiency-dependent combination of salinity and high light intensity could be capable of improving the high accumulation of valuable by-products such as canthaxanthin and astaxanthin rather than that of lutein when the algal cells of *S. rubescens* KNUA042 were cultured for 14 days and indicated that lutein production would be effective when the algal cells were challenged to N deficiency alone or high salinity coupled to high light intensity for 7 days. Furthermore, the obtained results showed that the desired products included lutein, canthaxanthin, and astaxanthin obtained by culture methods such as harvesting point and a stress-dependent mode.

5. Conclusions

Our results showed that N deficiency-dependent high salinity coupled to high light intensity in the TSC process minimized cellular damage and improved the enhanced production of lipids-derived biofuel materials (including C16:0 (palmitic acid), C18:1 (oleic acid) and C18:3 (linolenic acid)) and high-value products (such as carotenoids). In addition, under stress conditions, the algal strain accumulated β -carotene, astaxanthin isomers with lutein and canthaxanthin. Furthermore, our study provided the first evidence of the sequential co-production of carotenoids as well as biofuel feedstock in the *S. rubescens* KNUA042 strain by controlling stress type and culture method.

Supplementary Materials: The following are available online at <http://www.mdpi.com/2071-1050/12/13/5445/s1>, Figure S1: (A) Map of the study area, located on the East sea, Korea and light microscopy of *S. rubescens* KNUA042. Figure S2: Phylogenetic analysis of KNUA042 and its closely related species based on ITS2 region sequences. Figure S3: Phylogenetic analysis of KNUA042 and closely related species based on 18S rRNA sequences. Figure S4: Comparison of nitrate-N concentration, dry weight, and optical density in *S. rubescens* KNUA042 cells under different nitrate-N concentrations. Figure S5: Growth rate of *S. rubescens* KNUA042 cells under various stress conditions from day 0 to day 14. Figure S6: Thin layer chromatographic (TLC) analysis of total lipids in *S. rubescens* KNUA042 cells under different stress conditions on day 14 of cultivation. Figure S7: Microscopic image of stressed *S. rubescens* KNUA042 cells subjected to nitrogen deficiency (A, control), salinity (B), high light intensity (C), and combined (D, high light intensity + salinity) during the final days of cultivation. Figure S8: Comparison of chlorophyll *a* content, chlorophyll *b* content, total carotenoid content in different microalgae strains. Table S1: Results from BLAST searches using the sequences of 18S rRNA, ITS2, and *rbcL* genes of strain KNUA042.

Author Contributions: Conceptualization, S.-W.J., I.-S.K., and H.-S.Y.; methodology, S.-W.J., J.W.H., J.-M.D., and H.N.; formal analysis, S.-W.J., J.W.H., J.-J.K., and S.-I.P.; investigation, Y.-S.K.; writing—original draft preparation, S.-W.J., J.W.H., I.-S.K., and H.-S.Y.; writing—review and editing, Y.-S.K., I.-S.K., and H.-S.Y. All authors have read and agreed to the published version of the manuscript.

Funding: This research was supported by a grant from the National Research Foundation of Korea (NRF-2017R1A2B4002016) and the Next-Generation BioGreen 21 Program (No. PJ013240), Rural Development Administration, Korea.

Conflicts of Interest: The authors declare no conflict of interest.

References

1. Ho, S.H.; Chen, C.Y.; Chang, J.S. Effect of light intensity and nitrogen starvation on CO₂ fixation and lipid/carbohydrate production of an indigenous microalga *Scenedesmus obliquus* CNW-N. *Bioresour. Technol.* **2012**, *113*, 244–252. [[CrossRef](#)]
2. Guedes, A.G.P.; Morisseau, C.; Sole, A.; Soares, J.H.N.; Ulu, A.; Dong, H.; Hammock, B.D. Use of a soluble epoxide hydrolase inhibitor as an adjunctive analgesic in a horse with laminitis. *Vet. Anaesth. Analg.* **2013**, *40*, 440–448. [[CrossRef](#)] [[PubMed](#)]
3. Riccio, G.; Lauritano, C. Microalgae with immunomodulatory activities. *Mar. Drugs* **2020**, *18*, 2. [[CrossRef](#)] [[PubMed](#)]
4. Patnaik, R.; Singh, N.K.; Bagchi, S.K.; Rao, P.S.; Mallick, N. Utilization of *Scenedesmus obliquus* protein as a replacement of the commercially available fish meal under an algal refinery approach. *Front. Microbiol.* **2019**, *10*, 2114. [[CrossRef](#)] [[PubMed](#)]
5. Patil, L.; Kaliwal, B.B. Microalga *Scenedesmus bajacalifornicus* BBKLP-07, a new source of bioactive compounds with in vitro pharmacological applications. *Bioprocess Biosyst. Eng.* **2019**, *42*, 979–994. [[CrossRef](#)] [[PubMed](#)]
6. Guedes, A.C.; Amaro, H.M.; Malcata, F.X. Microalgae as sources of carotenoids. *Mar. Drugs* **2011**, *9*, 625–644. [[CrossRef](#)]
7. Boussiba, S. Carotenogenesis in the green alga *Haematococcus pluvialis*: Cellular physiology and stress response. *Physiol. Plant.* **2000**, *108*, 111–117. [[CrossRef](#)]
8. Demmig-Adams, B.; Adams, W.W. Food and photosynthesis: Antioxidants in photosynthesis and human nutrition. *Science* **2002**, *298*, 2149–2153. [[CrossRef](#)]
9. Chisti, Y. Constraints to commercialization of algal fuels. *J. Biotechnol.* **2013**, *167*, 201–214. [[CrossRef](#)]
10. Jebali, A.; Acién, F.G.; Jiménez-Ruiz, N.; Gómez, C.; Fernández-Sevilla, J.M.; Mhiri, N.; Karray, F.; Sayadi, S.; Molina-Grima, E. Evaluation of native microalgae from Tunisia using the pulse-amplitude-modulation measurement of chlorophyll fluorescence and a performance study in semi-continuous mode for biofuel production. *Biotechnol. Biofuels* **2019**, *12*, 119. [[CrossRef](#)]
11. Gong, M.; Bassi, A. Carotenoids from microalgae: A review of recent developments. *Biotechnol. Adv.* **2016**, *34*, 1396–1412. [[CrossRef](#)] [[PubMed](#)]
12. Singh, P.; Kumari, S.; Guldhe, A.; Misra, R.; Rawat, I.; Bux, F. Trends and novel strategies for enhancing lipid accumulation and quality in microalgae. *Renew. Sustain. Energy Rev.* **2016**, *55*, 1–16. [[CrossRef](#)]
13. Duan, X. Salt-induced osmotic stress for lipid overproduction in batch culture of *Chlorella vulgaris*. *African J. Biotechnol.* **2012**, *11*, 7072–7078. [[CrossRef](#)]
14. Takagi, M.; Karseno; Yoshida, T. Effect of salt concentration on intracellular accumulation of lipids and triacylglyceride in marine microalgae *Dunaliella* cells. *J. Biosci. Bioeng.* **2006**, *101*, 223–226. [[CrossRef](#)]
15. Coesel, S.N.; Baumgartner, A.C.; Teles, L.M.; Ramos, A.A.; Henriques, N.M.; Cancela, L.; Varela, J.C.S. Nutrient limitation is the main regulatory factor for carotenoid accumulation and for Psy and Pds steady state transcript levels in *Dunaliella salina* (Chlorophyta) exposed to high light and salt stress. *Mar. Biotechnol.* **2008**, *10*, 602–611. [[CrossRef](#)]
16. Ra, C.H.; Kang, C.H.; Kim, N.K.; Lee, C.G.; Kim, S.K. Cultivation of four microalgae for biomass and oil production using a two-stage culture strategy with salt stress. *Renew. Energy* **2015**, *80*, 117–122. [[CrossRef](#)]
17. Rippka, R.; Deruelles, J.; Waterbury, J.B.; Herdman, M.; Stanier, R.Y. Generic assignments, strain histories and properties of pure cultures of cyanobacteria. *Microbiology* **1979**, *111*, 1–61. [[CrossRef](#)]
18. White, T.J.; Bruns, T.; Lee, S.; Taylor, J. Amplification and direct sequencing of fungal ribosomal RNA Genes for phylogenetics. In *PCR Protocols: A Guide to Methods and Applications*; Department of Biological Sciences Louisiana State University: Baton Rouge, LA, USA, 1990; Volume 18, pp. 315–322.
19. Verbruggen, H.; Ashworth, M.; LoDuca, S.T.; Vlaeminck, C.; Cocquyt, E.; Sauvage, T.; Zechman, F.W.; Littler, D.S.; Littler, M.M.; Leliaert, F.; et al. A multi-locus time-calibrated phylogeny of the siphonous green algae. *Mol. Phylogenet. Evol.* **2009**, *50*, 642–653. [[CrossRef](#)]
20. Kumar, S.; Stecher, G.; Tamura, K. MEGA7: Molecular evolutionary genetics analysis version 7.0 for bigger datasets. *Mol. Biol. Evol.* **2016**, *33*, 1870–1874. [[CrossRef](#)]
21. Kang, Z.; Kim, B.H.; Ramanan, R.; Choi, J.E.; Yang, J.W.; Oh, H.M.; Kim, H.S. A cost analysis of microalgal biomass and biodiesel production in open raceways treating municipal wastewater and under optimum light wavelength. *J. Microbiol. Biotechnol.* **2015**, *25*, 109–118. [[CrossRef](#)]

22. Mishra, S.K.; Suh, W.I.; Farooq, W.; Moon, M.; Shrivastav, A.; Park, M.S.; Yang, J.W. Rapid quantification of microalgal lipids in aqueous medium by a simple colorimetric method. *Bioresour. Technol.* **2014**, *155*, 330–333. [[CrossRef](#)] [[PubMed](#)]
23. Given, P.H.; Weldon, D.; Zoeller, J.H. Calculation of calorific values of coals from ultimate analyses: Theoretical basis and geochemical implications. *Fuel* **1986**, *65*, 849–854. [[CrossRef](#)]
24. Breuer, G.; Evers, W.A.C.; de Vree, J.H.; Kleinegriss, D.M.M.; Martens, D.E.; Wijffels, R.H.; Lamers, P.P. Analysis of fatty acid content and composition in microalgae. *J. Vis. Exp.* **2013**, *80*, e50628. [[CrossRef](#)]
25. Govender, T.; Ramanna, L.; Rawat, I.; Bux, F. BODIPY staining, an alternative to the Nile Red fluorescence method for the evaluation of intracellular lipids in microalgae. *Bioresour. Technol.* **2012**, *114*, 507–511. [[CrossRef](#)]
26. Lichtenthaler, H.K.; Buschmann, C. Chlorophylls and carotenoids measurement and UV-VIS characterization. In *Current Protocols in Food Analytical Chemistry*; Wrolstad, R.E., Ed.; John Wiley and Sons Inc.: New York, NY, USA, 2001; pp. F4.3.1–F4.3.8. [[CrossRef](#)]
27. Zapata, M.; Garrido, J.L. Influence of injection conditions in reversed-phase high-performance liquid chromatography of chlorophylls and carotenoids. *Chromatographia* **1991**, *31*, 589–594. [[CrossRef](#)]
28. Sanz, N.; García-Blanco, A.; Gavalás-Olea, A.; Loures, P.; Garrido, J.L. Phytoplankton pigment biomarkers: HPLC separation using a pentafluorophenyl octadecyl silica column. *Methods Ecol. Evol.* **2015**, *6*, 1199–1209. [[CrossRef](#)]
29. Aussant, J.; Guihéneuf, F.; Stengel, D.B. Impact of temperature on fatty acid composition and nutritional value in eight species of microalgae. *Appl. Microbiol. Biotechnol.* **2018**, *102*, 5279–5297. [[CrossRef](#)]
30. Osundeko, O.; Davies, H.; Pittman, J.K. Oxidative stress-tolerant microalgae strains are highly efficient for biofuel feedstock production on wastewater. *Biomass Bioenergy* **2013**, *56*, 284–294. [[CrossRef](#)]
31. Yang, I.-S.; Salama, E.-S.; Kim, J.-O.; Govindwar, S.P.; Kurade, M.B.; Lee, M.; Roh, H.-S.; Jeon, B.-H. Cultivation and harvesting of microalgae in photobioreactor for biodiesel production and simultaneous nutrient removal. *Energy Convers. Manag.* **2016**, *117*, 54–62. [[CrossRef](#)]
32. Kessler, E.; Schäfer, M.; Hümmel, C.; Kloboucek, A.; Huss, V.A.R. Physiological, biochemical, and molecular characters for the taxonomy of the subgenera of *Scenedesmus* (Chlorococcales, Chlorophyta). *Bot. Acta* **1997**, *110*, 244–250. [[CrossRef](#)]
33. Awaluddin, S.A.; Thiruvenkadam, S.; Izhar, S.; Hiroyuki, Y.; Danquah, M.K.; Harun, R. Subcritical water technology for enhanced extraction of biochemical compounds from *Chlorella vulgaris*. *Biomed Res. Int.* **2016**, *5816974*. [[CrossRef](#)]
34. Hong, J.W.; Kim, O.H.; Jo, S.W.; Do, J.M.; Yoon, H.S. Microalgal biomass productivity and dominant species transition in a Korean mass cultivation system. *Algal Res.* **2017**, *26*, 365–370. [[CrossRef](#)]
35. Choi, G.G.; Kim, B.H.; Ahn, C.Y.; Oh, H.M. Effect of nitrogen limitation on oleic acid biosynthesis in *Botryococcus braunii*. *J. Appl. Phycol.* **2011**, *23*, 1031–1037. [[CrossRef](#)]
36. Hegewald, E.H. Taxonomy and phylogeny of *Scenedesmus*. *Algae* **1997**, *12*, 235–246.
37. Tan, Y.; Lin, J. Biomass production and fatty acid profile of a *Scenedesmus rubescens*-like microalga. *Bioresour. Technol.* **2011**, *102*, 10131–10135. [[CrossRef](#)]
38. Yilancioglu, K.; Cokol, M.; Pastirmaci, I.; Erman, B.; Cetiner, S. Oxidative stress is a mediator for increased lipid accumulation in a newly isolated *Dunaliella salina* strain. *PLoS ONE* **2014**, *9*, e91957. [[CrossRef](#)]
39. Orosa, M.; Torres, E.; Fidalgo, P.; Abalde, J. Production and analysis of secondary carotenoids in green algae. *J. Appl. Phycol.* **2000**, *12*, 553–556. [[CrossRef](#)]
40. Alishah Aratboni, H.; Rafiei, N.; Garcia-Granados, R.; Alemzadeh, A.; Morones-Ramírez, J.R. Biomass and lipid induction strategies in microalgae for biofuel production and other applications. *Microb. Cell Fact.* **2019**, *18*, 178. [[CrossRef](#)]
41. Abe, K.; Hattori, H.; Hirano, M. Accumulation and antioxidant activity of secondary carotenoids in the aerial microalga *Coelastrum striolatum* var. *multistriatum*. *Food Chem.* **2007**, *100*, 656–661. [[CrossRef](#)]
42. Simionato, D.; Block, M.A.; La Rocca, N.; Jouhet, J.; Maréchal, E.; Finazzi, G.; Morosinotto, T. The response of *Nannochloropsis gaditana* to nitrogen starvation includes de novo biosynthesis of triacylglycerols, a decrease of chloroplast galactolipids, and reorganization of the photosynthetic apparatus. *Eukaryot. Cell* **2013**, *12*, 665–676. [[CrossRef](#)]

43. Arguelles, E.D.; Laurena, A.C.; Monsalud, R.G.; Martinez-Goss, M.R. Fatty acid profile and fuel-derived physico-chemical properties of biodiesel obtained from an indigenous green microalga, *Desmodesmus* sp. (I-AU1), as potential source of renewable lipid and high quality biodiesel. *J. Appl. Phycol.* **2018**, *30*, 411–419. [[CrossRef](#)]
44. Sureshkumar, P.; Thomas, J. Strategic growth of limnic green microalgae with phycoremediation potential for enhanced production of biomass and biomolecules for sustainable environment. *Environ. Sci. Pollut. Res.* **2019**, *34*, 34702–34712. [[CrossRef](#)] [[PubMed](#)]
45. Sun, X.M.; Ren, L.J.; Zhao, Q.Y.; Ji, X.J.; Huang, H. Microalgae for the production of lipid and carotenoids: A review with focus on stress regulation and adaptation. *Biotechnol. Biofuels* **2018**, *11*, 272. [[CrossRef](#)] [[PubMed](#)]
46. Nayak, M.; Suh, W.I.; Chang, Y.K.; Lee, B. Exploration of two-stage cultivation strategies using nitrogen starvation to maximize the lipid productivity in *Chlorella* sp. HS2. *Bioresour. Technol.* **2019**, *276*, 110–118. [[CrossRef](#)] [[PubMed](#)]
47. Juan, P.; Kai, Y.; Jian Ping, Y.; Guang Xia, C.; Min, X.; Chou Fei, W.; Jiang Hai, W. Characterization of a newly isolated green microalga *Scenedesmus* sp. as a potential source of biodiesel. *African J. Biotechnol.* **2012**, *11*, 16083–16094. [[CrossRef](#)]
48. Sharma, T.; Gour, R.S.; Kant, A.; Chauhan, R.S. Lipid content in *Scenedesmus* species correlates with multiple genes of fatty acid and triacylglycerol biosynthetic pathways. *Algal Res.* **2015**, *12*, 341–349. [[CrossRef](#)]
49. Chokshi, K.; Pancha, I.; Ghosh, A.; Mishra, S. Salinity induced oxidative stress alters the physiological responses and improves the biofuel potential of green microalgae *Acutodesmus dimorphus*. *Bioresour. Technol.* **2017**, *244*, 1376–1383. [[CrossRef](#)]
50. Sun, H.; Mao, X.; Wu, T.; Ren, Y.; Chen, F.; Liu, B. Novel insight of carotenoid and lipid biosynthesis and their roles in storage carbon metabolism in *Chlamydomonas reinhardtii*. *Bioresour. Technol.* **2018**, *263*, 450–457. [[CrossRef](#)]
51. Salama, E.S.; Kim, H.C.; Abou-Shanab, R.A.I.; Ji, M.K.; Oh, Y.K.; Kim, S.H.; Jeon, B.H. Biomass, lipid content, and fatty acid composition of freshwater *Chlamydomonas mexicana* and *Scenedesmus obliquus* grown under salt stress. *Bioprocess Biosyst. Eng.* **2013**, *36*, 827–833. [[CrossRef](#)]
52. Sun, X.; Cao, Y.; Xu, H.; Liu, Y.; Sun, J.; Qiao, D.; Cao, Y. Effect of nitrogen-starvation, light intensity and iron on triacylglyceride/carbohydrate production and fatty acid profile of *Neochloris oleoabundans* HK-129 by a two-stage process. *Bioresour. Technol.* **2014**, *155*, 204–212. [[CrossRef](#)]
53. Steinbrenner, J.; Linden, H. Regulation of two carotenoid biosynthesis genes coding for phytoene synthase and carotenoid hydroxylase during stress-induced astaxanthin formation in the green alga *Haematococcus pluvialis*. *Plant Physiol.* **2001**, *125*, 810–817. [[CrossRef](#)]
54. Rumin, J.; Bonnefond, H.; Saint-Jean, B.; Rouxel, C.; Sciandra, A.; Bernard, O.; Cadoret, J.-P.; Bougaran, G. The use of fluorescent Nile red and BODIPY for lipid measurement in microalgae. *Biotechnol. Biofuels* **2015**, *8*, 42. [[CrossRef](#)] [[PubMed](#)]
55. Affenzeller, M.J.; Darehshouri, A.; Andosch, A.; Lütz, C.; Lütz-Meindl, U. Salt stress-induced cell death in the unicellular green alga *Micrasterias denticulata*. *J. Exp. Bot.* **2009**, *60*, 939–954. [[CrossRef](#)] [[PubMed](#)]
56. You, Z.; Zhang, Q.; Peng, Z.; Miao, X. Lipid droplets mediate salt stress tolerance in *parachlorella kessleri*. *Plant Physiol.* **2019**, *181*, 510–526. [[CrossRef](#)] [[PubMed](#)]
57. Hu, Q.; Sommerfeld, M.; Jarvis, E.; Ghirardi, M.; Posewitz, M.; Seibert, M.; Darzins, A. Microalgal triacylglycerols as feedstocks for biofuel production: Perspectives and advances. *Plant J.* **2008**, *54*, 621–639. [[CrossRef](#)]
58. Rodolfi, L.; Zittelli, G.C.; Bassi, N.; Padovani, G.; Biondi, N.; Bonini, G.; Tredici, M.R. Microalgae for oil: Strain selection, induction of lipid synthesis and outdoor mass cultivation in a low-cost photobioreactor. *Biotechnol. Bioeng.* **2009**, *102*, 100–112. [[CrossRef](#)]
59. Khozin-Goldberg, I.; Cohen, Z. The effect of phosphate starvation on the lipid and fatty acid composition of the fresh water eustigmatophyte *Monodus subterraneus*. *Phytochemistry* **2006**, *67*, 696–701. [[CrossRef](#)]
60. Kent, M.; Welladsen, H.M.; Mangott, A.; Li, Y. Nutritional evaluation of Australian microalgae as potential human health supplements. *PLoS ONE* **2015**, *10*, e0118985. [[CrossRef](#)]
61. Bi, Z.; He, B.B. Characterization of microalgae for the purpose of biofuel production. *ASABE* **2013**, *56*, 1529–1539.

62. Sukarni; Sudjito; Hamidi, N.; Yanuhar, U.; Wardana, I.N.G. Potential and properties of marine microalgae *Nannochloropsis oculata* as biomass fuel feedstock. *Int. J. Energy Environ. Eng.* **2014**, *5*, 279–290. [[CrossRef](#)]
63. Ross, A.B.; Jones, J.M.; Kubacki, M.L.; Bridgeman, T. Classification of macroalgae as fuel and its thermochemical behaviour. *Bioresour. Technol.* **2008**, *99*, 6494–6504. [[CrossRef](#)] [[PubMed](#)]
64. Halim, R.; Gladman, B.; Danquah, M.K.; Webley, P.A. Oil extraction from microalgae for biodiesel production. *Bioresour. Technol.* **2011**, *102*, 178–185. [[CrossRef](#)] [[PubMed](#)]
65. Ho, S.-H.; Nakanishi, A.; Ye, X.; Chang, J.-S.; Hara, K.; Hasunuma, T.; Kondo, A. Optimizing biodiesel production in marine *Chlamydomonas* sp. JSC4 through metabolic profiling and an innovative salinity-gradient strategy. *Biotechnol. Biofuels* **2014**, *7*, 97. [[CrossRef](#)]
66. Solovchenko, A.E.; Khozin-Goldberg, I.; Didi-Cohen, S.; Cohen, Z.; Merzlyak, M.N. Effects of light intensity and nitrogen starvation on growth, total fatty acids and arachidonic acid in the green microalga *Parietochloris incisa*. *J. Appl. Phycol.* **2007**, *20*, 245–251. [[CrossRef](#)]
67. Lin, Q.; Lin, J. Effects of nitrogen source and concentration on biomass and oil production of a *Scenedesmus rubescens* like microalga. *Bioresour. Technol.* **2011**, *102*, 1615–1621. [[CrossRef](#)] [[PubMed](#)]
68. Mandotra, S.K.; Kumar, P.; Suseela, M.R.; Ramteke, P.W. Fresh water green microalga *Scenedesmus abundans*: A potential feedstock for high quality biodiesel production. *Bioresour. Technol.* **2014**, *156*, 42–47. [[CrossRef](#)] [[PubMed](#)]
69. Shen, P.L.; Wang, H.T.; Pan, Y.F.; Meng, Y.Y.; Wu, P.C.; Xue, S. Identification of characteristic fatty acids to quantify triacylglycerols in microalgae. *Front. Plant Sci.* **2016**, *7*, 162. [[CrossRef](#)]
70. Liu, J.; Yuan, C.; Hu, G.; Li, F. Effects of light intensity on the growth and lipid accumulation of microalga *Scenedesmus* sp. 11-1 under nitrogen limitation. *Appl. Biochem. Biotechnol.* **2012**, *166*, 2127–2137. [[CrossRef](#)]
71. Xia, L.; Ge, H.; Zhou, X.; Zhang, D.; Hu, C. Photoautotrophic outdoor two-stage cultivation for oleaginous microalgae *Scenedesmus obtusus* XJ-15. *Bioresour. Technol.* **2013**, *144*, 261–267. [[CrossRef](#)]
72. Minhas, A.K.; Hodgson, P.; Barrow, C.J.; Adholeya, A. A review on the assessment of stress conditions for simultaneous production of microalgal lipids and carotenoids. *Front. Microbiol.* **2016**, *7*, 546. [[CrossRef](#)]
73. He, Q.; Yang, H.; Hu, C. Effects of temperature and its combination with high light intensity on lipid production of *Monoraphidium dybowskii* Y2 from semi-arid desert areas. *Bioresour. Technol.* **2018**, *265*, 407–414. [[CrossRef](#)] [[PubMed](#)]
74. Talebi, A.F.; Mohtashami, S.K.; Tabatabaei, M.; Tohidfar, M.; Bagheri, A.; Zeinalabedini, M.; Hadavand Mirzaei, H.; Mirzajanzadeh, M.; Malekzadeh Shafaroudi, S.; Bakhtiari, S. Fatty acids profiling: A selective criterion for screening microalgae strains for biodiesel production. *Algal Res.* **2013**, *2*, 258–267. [[CrossRef](#)]
75. Pal, D.; Khozin-Goldberg, I.; Cohen, Z.; Boussiba, S. The effect of light, salinity, and nitrogen availability on lipid production by *Nannochloropsis* sp. *Appl. Microbiol. Biotechnol.* **2011**, *90*, 1429–1441. [[CrossRef](#)] [[PubMed](#)]
76. He, Q.; Yang, H.; Wu, L.; Hu, C. Effect of light intensity on physiological changes, carbon allocation and neutral lipid accumulation in oleaginous microalgae. *Bioresour. Technol.* **2015**, *191*, 219–228. [[CrossRef](#)]

